CONFIDENTIAL

NASA TM X-571

TECHNICAL MEMORANDUM

X-571

THE LONGITUDINAL AERODYNAMIC CHARACTERISTICS OF A RE-ENTRY CONFIGURATION BASED ON A BLUNT 13° HALF-CONE AT MACH NUMBERS TO 0.92

By George C. Kenyon and Fred B. Sutton

Ames Research Center
Moffett Field, Calif.

NATIONAL AERONAUTICS AND SPACE ADMINISTRATION

WASHINGTON

July 1961

CONFIDENTIAL

NATIONAL AERONAUTICS AND SPACE ADMINISTRATION

TECHNICAL MEMORANDUM X-571

THE LONGITUDINAL AERODYNAMIC CHARACTERISTICS OF A RE-ENTRY CONFIGURATION BASED ON A BLUNT 13° HALF-CONE AT MACH NUMBERS TO 0.92*

By George C. Kenyon and Fred B. Sutton

SUMMARY

A wind-tunnel investigation has been made to evaluate the subsonic aerodynamic characteristics of a lifting-body re-entry configuration based on a 13° half-cone. This report presents the performance and longitudinal stability and control characteristics of the model at Mach numbers from 0.25 to 0.92. The tests were conducted at Reynolds numbers up to 25 million based on model length at a Mach number of 0.25 and at a Reynolds number of 5 million for Mach numbers varying from 0.60 to 0.92.

The test results show that with the appropriate combination of controls, the model had nearly linear lift and pitching-moment curves and static longitudinal stability (about a moment center at 55 percent of the length) to lift coefficients greater than 1.0 at low speed (M = 0.25). At Mach numbers from 0.60 to 0.92, these favorable characteristics prevailed to lift coefficients in excess of those required for steady level flight of a hypothetical vehicle with the model configuration. At low speed, a combination of outboard elevons and an upper surface trailing-edge flap provided satisfactory longitudinal stability and trimmed the model at lift coefficients from 0.2 to 0.6 with corresponding lift-drag ratios in excess of 3.0. The maximum trim lift-drag ratio at low speeds was about 4.0. The outboard elevons in combination with flaps on the rear lower surface of the body provided satisfactory longitudinal stability and control at high subsonic speeds. It is concluded that the performance and longitudinal stability and control of a full-scale vehicle having the test configuration would be adequate for a horizontal landing.

*Title, Unclassified

INTRODUCTION

The Ames Research Center has engaged in a research program to study the characteristics of lifting bodies based on a blunt 13° half-cone and to study their suitability for re-entry vehicles. In the investigation of reference 1, it has been shown that such vehicles can attain lift-drag ratios of about 1.5 at hypersonic speeds, providing lateral range capability of about 1000 miles when re-entry is accomplished from satelite orbit. Also, an investigation of the subsonic aerodynamic characteristics of modified blunt 13° half-cones (ref. 2) has indicated the possibility that such a vehicle could be provided with horizontal landing capability.

The information from these preliminary investigations has been used to guide the selection of a new study configuration for additional testing at subsonic, supersonic, and hypersonic speeds. The new configuration includes such features as thick, slab-sided control surfaces with comparatively large leading-edge radii, local flattening of the sides and bottom of the body at the rear for mounting control surfaces, lower surface flaps for stability and control, and side-mounted flaps for yaw control and speed braking. Reference 3 presents some preliminary results obtained at subsonic and supersonic speeds and reference 4 documents the complete results to date obtained at supersonic speeds.

The present report contains the results of tests performed in the Ames 12-Foot Pressure Wind Tunnel, concurrent with those reported in reference 4, to evaluate the subsonic static longitudinal aerodynamic characteristics of this new re-entry configuration. The experiments covered a Mach number range from 0.25 to 0.92.

Tests at a Mach number of 0.25 were conducted primarily at a Reynolds number of 15 million based on model length; however, some tests at this Mach number were conducted over a Reynolds number range from 1 million to 25 million. Tests at Mach numbers from 0.60 to 0.92 were conducted at a Reynolds number of 5 million. Longitudinal control effectiveness was measured for the outboard elevons, an upper surface trailing-edge flap, and pitch flaps mounted on the underside of the body. Also evaluated were the effects of the side-mounted flaps functioning as speed brakes and the effects of a typical landing-gear installation. The report includes the results of an analysis of the landing performance of a hypothetical vehicle based on the test configuration.

NOTATION

The results of the investigation are presented in the form of standard coefficients of forces and moments and are referred to the conventional stability axes. The moment center for the model was located at 55 percent of the length from the nose and 7 percent of the length below the cone axis. The coefficients and symbols used are defined as follows:

C_D drag coefficient, $\frac{\text{drag}}{qS}$

C_L lift coefficient, $\frac{\text{lift}}{qS}$

C_m pitching-moment coefficient, $\frac{\text{pitching moment}}{q\ell S}$

C_p base-pressure coefficient, $\frac{p_b - p}{q}$

$\frac{L}{D}$ lift-drag ratio, $\frac{\text{lift}}{\text{drag}}$

ℓ body length

M free-stream Mach number

p free-stream static pressure

p_b base pressure

q free-stream dynamic pressure

R Reynolds number, based on model length

S body plan-form area

V velocity

α angle of attack, referenced to cone axis

δ_e elevon deflection, positive with trailing edge down, measured from plane parallel to cone axis

δ_f trailing-edge flap deflection, positive with trailing edge down, measured from tangent to upper surface at the base

δ_p pitch flap deflection, positive with trailing edge down, measured from tangent to lower surface of the model

δ_{sb} speed brake deflection, measured from the side of the model

$\frac{\Delta C_m}{\Delta S}$ longitudinal control-effectiveness parameter at constant angle of attack

Subscripts

II initial point of phase II for the landing maneuver

III initial point of phase III for the landing maneuver

MODEL

The selection of geometric characteristics of the model was based on the results of references 1 and 2 and some additional considerations of structural and heating requirements for re-entry vehicles. Geometric properties of the model are given in figure 1, and photographs are presented in figure 2. The body was very similar in profile and plan form to body 4 of reference 2 but differed in cross section in the region of the boattail and in the profile of the blunt nose. The shape of the lower portion of the nose was changed from spherical on the reference model to a power series profile to eliminate the abrupt change in radius of curvature at the juncture of the nose and the conical section. The sides and bottom of the boattailed section were flattened to accommodate control surfaces that would produce pitching moments and yawing moments with low cross coupling. The vertical surfaces that extend above the body (vertical fins) provide flat mounting surfaces for the outboard elevons. The areas of the vertical fins and elevons were increased over those of the configuration of reference 2 and the cross sections of these surfaces were modified to have slab sides and increased leading-edge radii with a corresponding increase in thickness. The blunt trailing edges of these surfaces resulted in an increase in model base area from 17 percent of the plan-form area for the reference model to about 22 percent for the present model.

The model was equipped with three sets of movable surfaces for longitudinal control. These controls consisted of the outboard elevons, a trailing-edge flap extending from the upper surface, and a pair of flaps mounted on the rear lower surface. The total plan-form areas of these surfaces, in percent of body plan-form area, were 8.8, 10.1, and 5.8, respectively. The trailing-edge flap extending from the upper surface is referred to hereinafter as the trailing-edge flap and the lower surface flaps are referred to as pitch flaps. The model was also fitted

with yaw flaps mounted on the sides of the body and canted 15° to the cone axis so that they would be approximately alined with the stream at the angle for maximum L/D in hypersonic flight. The yaw flaps could be used as speed brakes when deflected simultaneously on each side of the body and are referred to as such in this report. A simulated landing gear consisted of a pair of skids and a nose wheel and is shown in figures 1(b) and 2(d).

The model was constructed of wood, fitted around a steel inner structure that incorporated a mounting for the six-component strain-gage balance. An orifice for measuring base pressure was located just inside the balance cavity, adjacent to the 2.5-inch-diameter sting. The model was painted with lacquer and hand rubbed with No. 400 sandpaper to a smooth finish.

A 4 8 3

TESTS

The longitudinal characteristics of the model were investigated over a range of Mach numbers from 0.25 to 0.92. Lift, drag, pitching moment, and base pressure were measured. Tests at a Mach number of 0.25 were conducted primarily at a Reynolds number of 15 million based on model length (37 in.); however, some tests at this Mach number were conducted over a Reynolds number range of 1 million to 25 million. Tests at Mach numbers of 0.60 to 0.92 were conducted at a Reynolds number of 5 million. The angle-of-attack range extended from -8° to +18° at most Mach numbers. The model was tested at all Mach numbers with the elevons, pitch flaps, and speed brakes at various angles of deflection and with the elevons off. Tests were also conducted at a Mach number of 0.25 with and without the trailing-edge flap and the landing gear.

CORRECTIONS TO DATA

The data have been corrected for constriction effects due to the tunnel walls by the method of reference 5. No corrections were made for tunnel-wall interference originating from lift on the model because calculations of this effect showed it to be negligible. Drag data are presented as measured, without adjustment for base pressure.

The corrections to Mach number and dynamic pressure due to constriction effects were as follows:

Corrected Mach No.	Uncorrected Mach No.	$\frac{q_{corrected}}{q_{uncorrected}}$
0.25	0.25	1.003
.60	.598	1.004
.70	.698	1.005
.80	.795	1.008
.85	.843	1.010
.90	.888	1.015
.92	.905	1.020

RESULTS AND DISCUSSION

Tests at Low Speed (M = 0.25)

The model was equipped with three separate sets of adjustable surfaces to provide longitudinal control throughout the test speed range. The basic low-speed characteristics of the model with various amounts of control deflection are presented in figures 3, 4, and 5 for a Mach number of 0.25 and a Reynolds number of 15 million. Figure 3 shows the effects of elevon deflection, figure 4 shows the effects of trailing-edge flap deflection, and figure 5 shows the effects of pitch-flap deflection. The moment center was located at 55 percent of the length from the nose and 7 percent of the length below the cone axis. The data show that the model was longitudinally stable, that the lift and pitching-moment curves were nearly linear, and that the model could be trimmed at lift coefficients from 0.2 to 0.6 with lift-drag ratios ranging from 3 to 4. The maximum lift-drag ratios for given control deflections were reached at lift coefficients between 0.4 and 0.5.

Figure 6 presents a comparison of the pitching-moment contributions of the elevons and of the trailing-edge flap at 0° deflection. The elevons provided a considerable increment of longitudinal stability as evidenced by the slope of the curve ΔC_m vs. α. Figure 6 also presents a comparison of the control-effectiveness parameter $\Delta C_m/\Delta\delta$ for the three sets of longitudinal control surfaces; the elevons, the trailing-edge flap, and the pitch flap. The data indicate that the effectiveness of each of the controls remained nearly constant throughout the angle-of-attack range. While the pitch flaps were intended primarily for control at high speeds, they provide some degree of control at low speeds with an insignificant effect on the drag.

Figure 7 presents a comparison of the aerodynamic characteristics of the current configuration with those of an earlier configuration developed in the preliminary investigation reported in reference 2. The

maximum lift-drag ratio of about 4 for the current model is considerably less than the value of about 6 for the reference model but is still well above the value of 2.5 that has been suggested in reference 6 as a minimum requirement for a horizontal landing. The increase in drag at low lift coefficients that caused this reduction in lift-drag ratio can be partially attributed to the increase in base area (from 17 percent of the plan area for the reference model to 22 percent for the current model) and the reduced pressure recovery at the base. However, it should be noted that the drag characteristics (and consequently the lift-drag ratio) were slightly improved at the higher lift coefficients.

The effects of extending the yaw controls symmetrically as speed brakes are shown in figure 8. Deflecting the speed brakes to 40° more than doubled the minimum drag and reduced the trim angle of attack by 3° for the longitudinal control settings shown ($\delta_e = -10°$, $\delta_f = -10°$, $\delta_p = 0°$). Deflecting the speed brakes had very little effect on the stability. With a small reorientation of the hinge lines of the speed brakes to reduce the trim change, it appears that speed brakes could provide a full-sized vehicle with good glide-path control.

A 4 8 3

The effects of a typical landing gear installation (see figs. 1(b) and 2(d)) on the longitudinal characteristics are shown in figure 9 for angles of attack to 30°. The addition of the landing gear had only minor effects on the performance and stability of the model; the lift and pitching-moment curves remained essentially linear throughout the angle-of-attack range.

Figure 10 presents the results of a survey of the effects of varying the Reynolds number, from 1 million to 25 million, on the longitudinal characteristics of the model. A Reynolds number of 25 million is nearly full scale for a 1/6-scale model. Figure 10(c) shows the nonlinearity that develops in the pitching-moment curves at low lift coefficients in the low Reynolds number range, probably as a result of separation of the boundary layer on the lower surface. The effects of Reynolds number are summarized in figure 11. It is apparent that increasing Reynolds number had little effect at Reynolds numbers greater than about 8 million.

Tests at High Speed (M = 0.60 to 0.92)

All the measurements at high subsonic speeds were made at a Reynolds number of 5 million. The high-speed data are presented for the model with the trailing-edge flap removed.

The longitudinal aerodynamic characteristics of the model with various deflections of the pitch flaps ranging from 0° (retracted) to 45° are presented for -10° elevon deflection in figure 12, for 0° elevon

deflection in figure 13, and for the model without elevons in figure 14. The data show that, in general, the lift and moment curves were nearly linear at Mach numbers of 0.60 and 0.70, but that at higher Mach numbers a sudden unstable trend in pitching moment developed, along with a loss in the lift-curve slope. The unstable break in the pitching-moment curves was delayed to progressively higher lift coefficients by increasing the pitch-flap deflection. The elevons provided a considerable increment of longitudinal stability as may be seen by comparing the pitching-moment curves of figure 14(c) (elevons off) with those of figures 12(c) and 13(c). The data of figure 12 show that with the elevons at -10° the model was longitudinally stable and, by modulating the pitch flaps, could be trimmed to lift coefficients ranging from about 0.6 at a Mach number of 0.60 to about 0.4 at a Mach number of 0.92.

The effects of Mach number variation on the longitudinal characteristics of the model, with the pitch flaps deflected 30°, are summarized in figure 15. The critical Mach number for the configuration appears to be about 0.9 as evidenced by the abrupt changes in the lift, drag, and pitching-moment characteristics that occurred at this Mach number.

Figure 16 presents the control-effectiveness parameter, $\Delta C_m/\Delta\delta$, for the elevons and pitch flaps, as a function of angle of attack. Generally, the control effectiveness as a function of angle of attack was much more erratic for the elevons (fig. 16(a)) than for the pitch flaps (fig. 16(b)). The pitching-moment contributions of the elevons are presented in figure 17. Figure 18 shows the effect of Mach number variations on the longitudinal control effectiveness of the elevons and of the pitch flaps for a lift coefficient of 0.3.

Figure 19 presents a comparison for Mach numbers of 0.60 and 0.90 of some of the data of figures 12 and 14 with data from reference 4 obtained with a similar model at much lower Reynolds numbers. The data for the present model with a pitch-flap deflection of 35° were obtained by interpolation of the data of figures 12 and 14. The comparison shows good agreement between the two tests with the exception of the data for the 0° pitch-flap deflection at a Mach number of 0.90. Although the cause of this discrepancy is not known, it could result from the difference in Reynolds numbers (5 million for the present tests compared with 0.6 million) or the effects of different sting diameters (0.068ℓ for the present tests compared with 0.14ℓ). Since deflecting the pitch flaps essentially eliminated the discrepancy, it is suspected that there were major differences in the flow on the lower surface of the boat-tailed body in the region of the pitch flaps when the flaps were retracted. At a Mach number of 0.90, it is likely that local shock waves exist on this surface (flaps retracted) and their position, strength, and effect on the boundary layer could be affected by Reynolds number or sting interference. Deflection of the pitch flaps grossly alters the body shape in this region, tending to fix the position of local shock formations regardless of Reynolds number and possibly masking sting interference.

Figure 20 shows the effects of deflecting the yaw controls as speed brakes on the longitudinal characteristics of the model at Mach numbers from 0.60 to 0.90. The results are similar to those obtained at low speeds (fig. 8) in that deflecting the speed brakes 40° about doubled the minimum drag. However, in contrast to the results obtained at low speeds, the data for the high-speed tests show a slight decrease in stability and quite large changes in trim due to extending the speed brakes. The deflection angles shown are perhaps too extreme; it is estimated that a speed brake deflection of 10° would produce a 20-percent increase in drag at lift coefficients of about 0.2. With limitation of the speed brake deflection to lower angles and, as suggested previously, reorientation of the hinge line, it appears that the speed brakes could provide effective glide path control for a full-scale vehicle.

A 4 8 3

Longitudinal Performance of an Assumed Re-entry Vehicle

Horizontal flight.- In reference 6, the initial phase of recovery of a re-entry vehicle was assumed to begin at the completion of the re-entry phase, that is, at an altitude of 100,000 feet and a Mach number of 5. The recovery phase was assumed to be terminated at an altitude of 30,000 feet and at a subsonic Mach number. If a hypothetical re-entry vehicle, based on the model configuration, is assumed to have a source of thrust sufficient to maintain level flight at this lower altitude, it is of interest to examine the stability and performance indicated from the data that have been presented. Some longitudinal aerodynamic characteristics of such a hypothetical vehicle in steady level flight at 30,000 feet are presented in figure 21, assuming a plan form loading of 65 pounds per square foot. Lift coefficient, static longitudinal stability at trim, pitch-flap angle for trim, and trimmed lift-drag ratio are presented as functions of Mach number. It may be seen that the lift coefficients for level flight range from about 0.4 at a Mach number of 0.60 to less than 0.2 at a Mach number of 0.92, and that the vehicle would have static longitudinal stability and adequate control throughout this Mach number range. These lift coefficients are well below those at which longitudinal instability is indicated in figure 12. The data of figure 12 show that the model was longitudinally stable and could be trimmed to lift coefficients ranging from about 0.6 at a Mach number of 0.60 to about 0.4 at a Mach number of 0.92. Thus it appears that considerable margin in lift coefficient would be available for maneuvering below the limits imposed by longitudinal instability. If the hypothetical re-entry vehicle were considered to be without a source of thrust, the descent from altitude would be made at lift coefficients slightly less than those shown for steady level flight and therefore the margin for maneuvering would be even greater.

Horizontal landing capability.- A power-off landing-approach maneuver was calculated for the assumed re-entry vehicle using the test results and the technique for landing unpowered vehicles with low lift-drag ratios described in reference 7. The maneuver consists of three phases: Phase I is a high-speed descent from altitude aimed at a ground reference point short of the runway; Phase II is a constant "g" pull-out beginning at a specified speed and altitude and ending with the start of Phase III which is a shallow flight path along which the vehicle decelerates to the touchdown point. The calculation is a step procedure beginning at the touchdown point and working backward along the flight path. The following assumptions were made; plan-form loading of 65 pounds per square foot, lift coefficient of 0.6 at touchdown, flight-path angle of 3° during Phase III, a maximum lift coefficient of 0.4 during Phase II, and a normal acceleration of 2.2 g during Phase II. In addition, on the advice of the pilot who flew the tests reported in reference 7, Phase III was limited to 20 seconds duration which has the advantage of locating the aiming point close to the point of touchdown. During the reference investigation it was necessary to extend Phase III (with a consequent increase in the time duration of Phase III) to a high enough altitude to permit safe ejection if the final phase could not be entered with sufficient speed. With the development of safe low-level ejection capability, this altitude requirement need not be imposed and the optimum time duration of Phase III can be selected.

A 4 8 3

Figure 22(a) presents, for comparison, the calculated approach path that was considered the optimum for the test airplane in the reference investigation. Figure 22(b) presents two landing-approach patterns for the hypothetical re-entry vehicle of this investigation. The two patterns may be considered extremes. The first, with a relatively shallow dive angle (26.5°), was computed for the vehicle with speed brakes retracted, and therefore drag modulation could only steepen the flight-path angle. The second path, with a relatively steep dive angle (45°), was computed for the vehicle with a 20-percent increase in drag, requiring speed brake deflection ranging from about 10° for Phase I to about 30° for Phase III (assuming no trim change with deflection of the speed brakes). The two examples presented show that a landing-approach pattern could be computed incorporating a moderate approach angle in Phase I with plus and minus glide path control.

It is interesting to note that the velocity at touchdown for the assumed vehicle was 10 knots less than that for the reference airplane. Touchdown would be accomplished at an angle of attack of 15° and a lift coefficient of 0.6, well below the maximum lift coefficient. From a comparison of parts (a) and (b) of figure 22, it appears that the performance of the assumed vehicle would be adequate for horizontal landing.

CONCLUSIONS

A wind-tunnel investigation has been conducted at subsonic Mach numbers varying from 0.25 to 0.92 to measure the aerodynamic characteristics of a lifting-body re-entry configuration based on a 13° half-cone. This report presents the longitudinal characteristics of the vehicle with the following conclusions:

1. At low speed (M = 0.25) and large-scale Reynolds numbers, the test results show that, with a combination of elevons and a trailing-edge flap, the model had nearly linear lift and pitching-moment curves to lift coefficients in excess of 1.0, static longitudinal stability about a moment center at 55 percent of the length, and a maximum trimmed lift-drag ratio of about 4. The model could be trimmed at lift coefficients ranging from about 0.2 to 0.6 with corresponding trimmed lift-drag ratios above 3.

A 4 8 3

2. At high subsonic speeds (M = 0.60 to 0.92), the test results show that with a combination of elevons and pitch flaps, the model had nearly linear lift and pitching-moment curves to lift coefficients well in excess of those required for steady level flight of a hypothetical vehicle with the model configuration. The model had static longitudinal stability about the chosen moment center and could be trimmed through the lift coefficient range of interest for steady level flight at high subsonic speeds.

3. Side-mounted yaw-control flaps proved effective as speed brakes when deflected symmetrically, providing good glide path control for an assumed vehicle. However, a small reorientation of the flap hinge lines would be desirable to eliminate trim changes with flap deflection.

4. A hypothetical re-entry vehicle based on the model configuration with a wing loading of 65 pounds per square foot appears to have adequate performance and static-longitudinal stability and control for a horizontal landing.

Ames Research Center
National Aeronautics and Space Administration
Moffett Field, Calif., May 4, 1961

REFERENCES

1. Rakich, John V.: Supersonic Aerodynamic Performance and Static-Stability Characteristics of Two Blunt-Nosed Modified 13° Half-Cone Configurations. NASA TM X-375, 1960.

2. Kenyon, George C., and Edwards, George G.: A Preliminary Investigation of Modified Blunt 13° Half-Cone Re-entry Configurations at Subsonic Speeds. NASA TM X-501, 1961.

3. Dennis, David H., and Edwards, George G.: The Aerodynamic Characteristics of Some Lifting Bodies. NASA TM X-376, 1960.

4. Rakich, John V.: Aerodynamic Performance and Static-Stability Characteristics of a Blunt-Nosed Boattailed 13° Half-Cone at Mach Numbers From 0.6 to 5.0. NASA TM X-570, 1961.

5. Herriot, John G.: Blockage Corrections for Three-Dimensional-Flow Closed Throat Wind Tunnels With Consideration of the Effect of Compressibility. NACA Rep. 995, 1950 (Supersedes NACA RM A7B28).

6. Weil, Joseph, and Matranga, Gene J.: Review of Techniques Applicable to the Recovery of Lifting Hypervelocity Vehicles. NASA TM X-334, 1960.

7. Bray, Richard S., Drinkwater, Fred J., III, and White, Maurice D.: A Flight Study of a Power-Off Landing Technique Applicable to Re-entry Vehicles. NASA TN D-323, 1960.

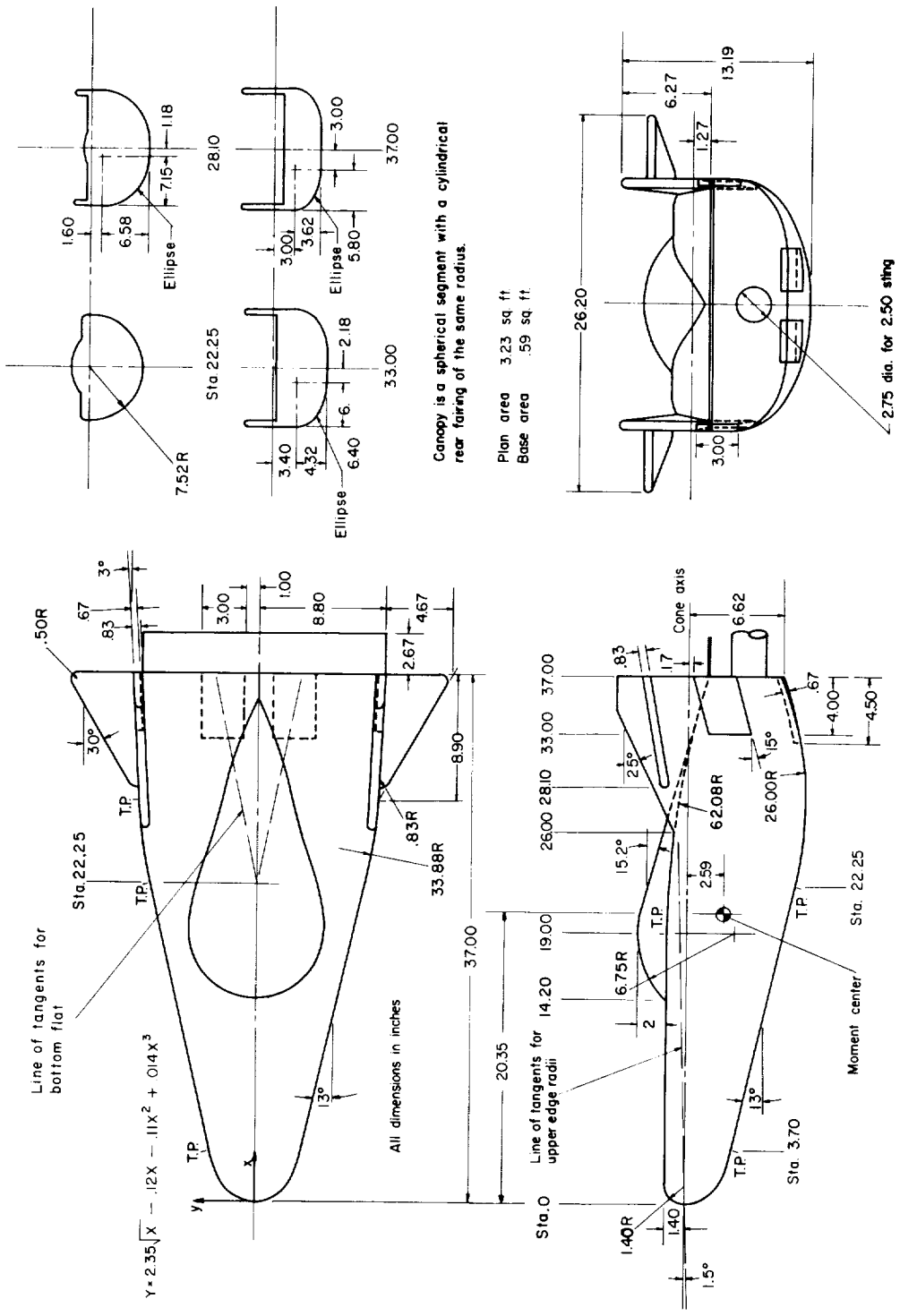

(a) General arrangement

Figure 1.- Geometry of the model.

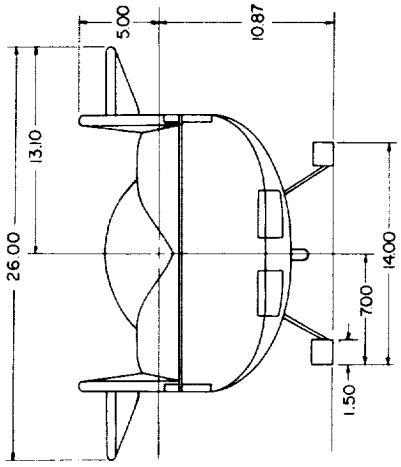

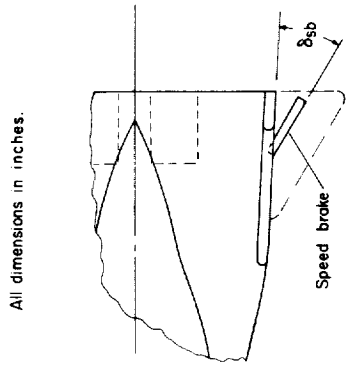

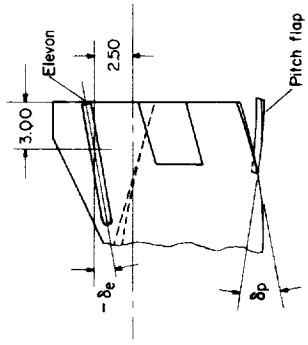

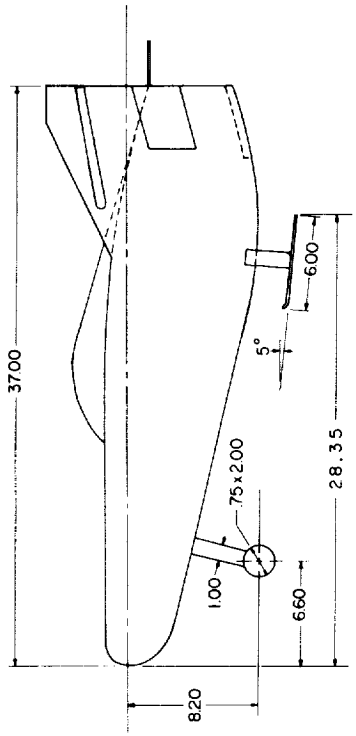

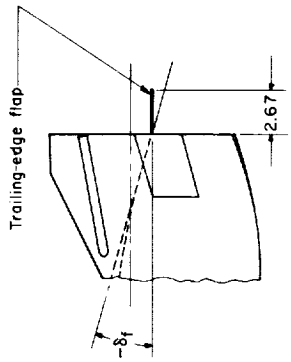

(b) Model details.

Figure 1.- Concluded.

A 4 8 3

A-27096

(a) Pitch flaps and speed brakes closed, trailing-edge flap off.

Figure 2.- Photographs of the model.

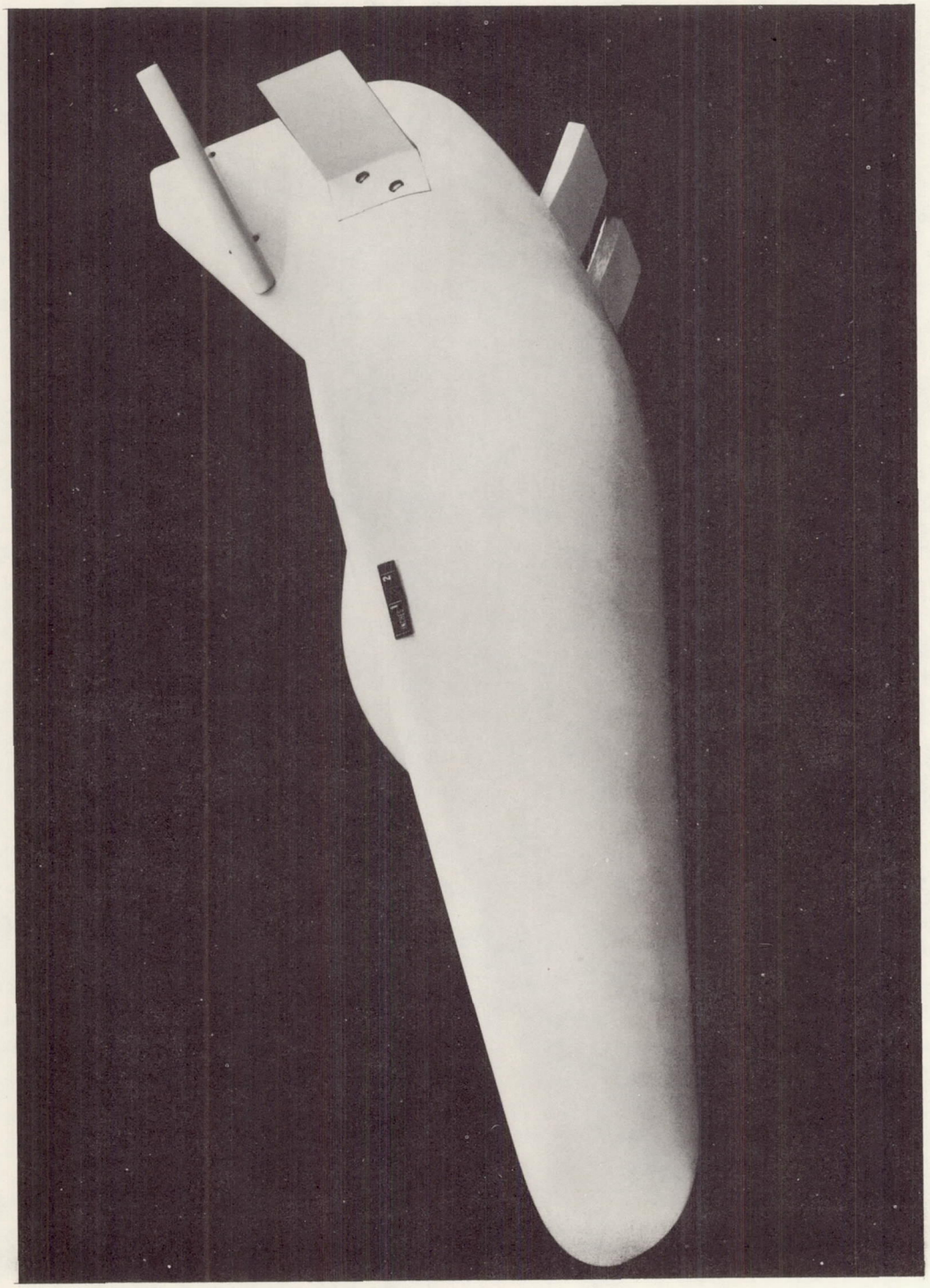

A-26178

(b) Pitch flaps and speed brakes open.

Figure 2.- Continued.

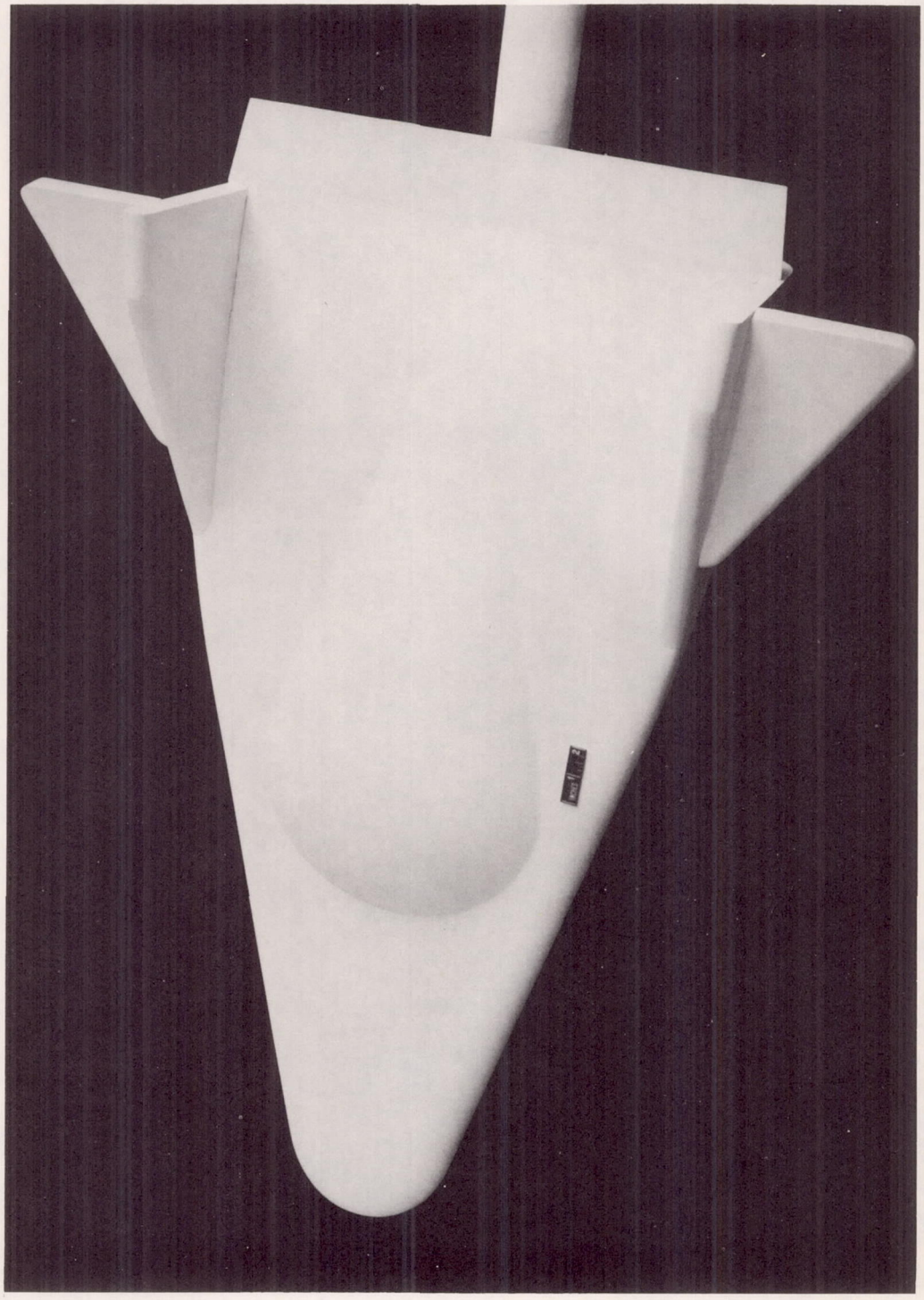

A-27094

(c) Trailing-edge flap on.

Figure 2.- Continued.

A-26359

(d) Landing gear extended.

Figure 2.- Concluded.

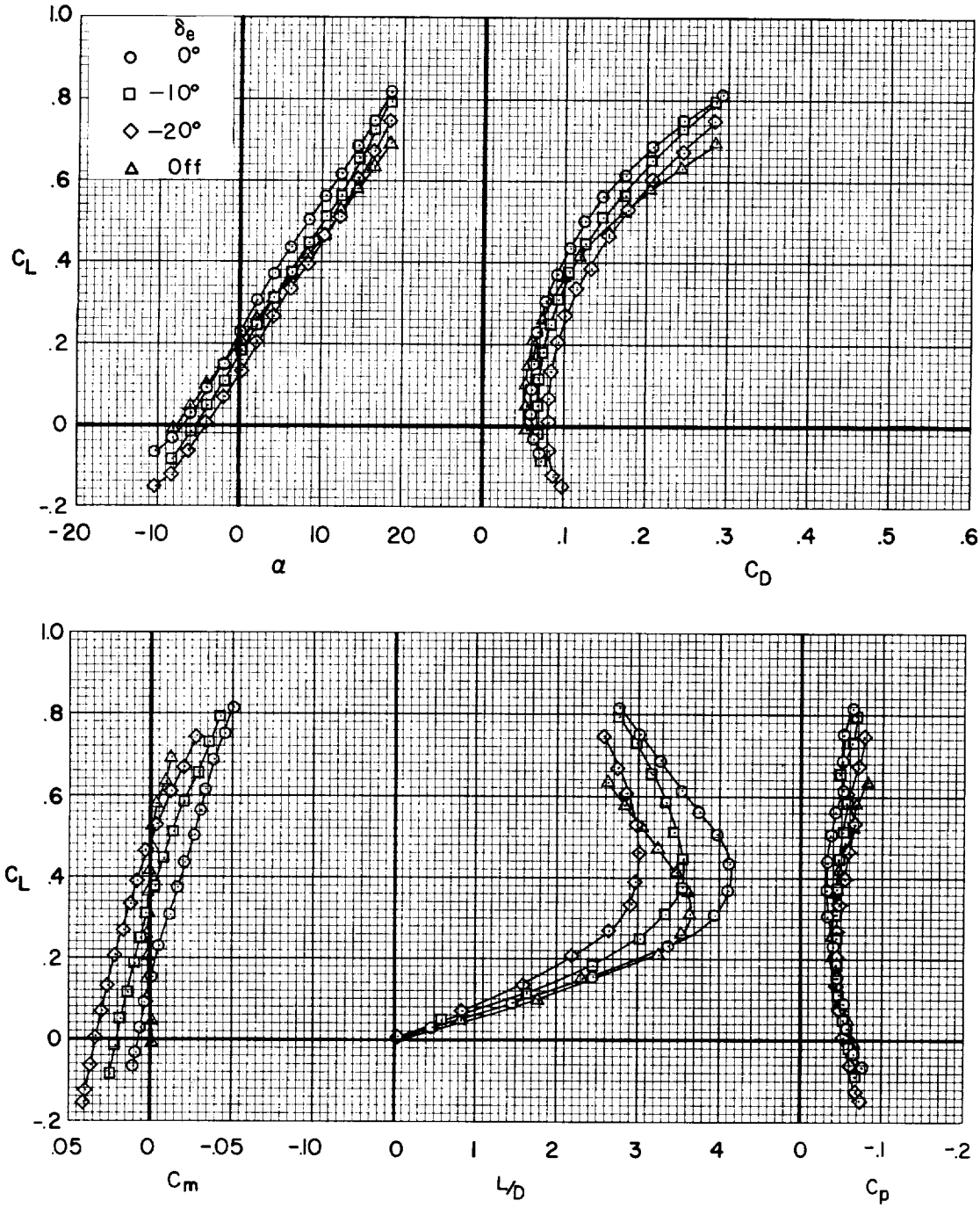

(a) $\delta_f = 0°$

Figure 3.- The effects of elevon deflection on the longitudinal characteristics of the model; M = 0.25, R = 15×10^6, $\delta_p = 0°$.

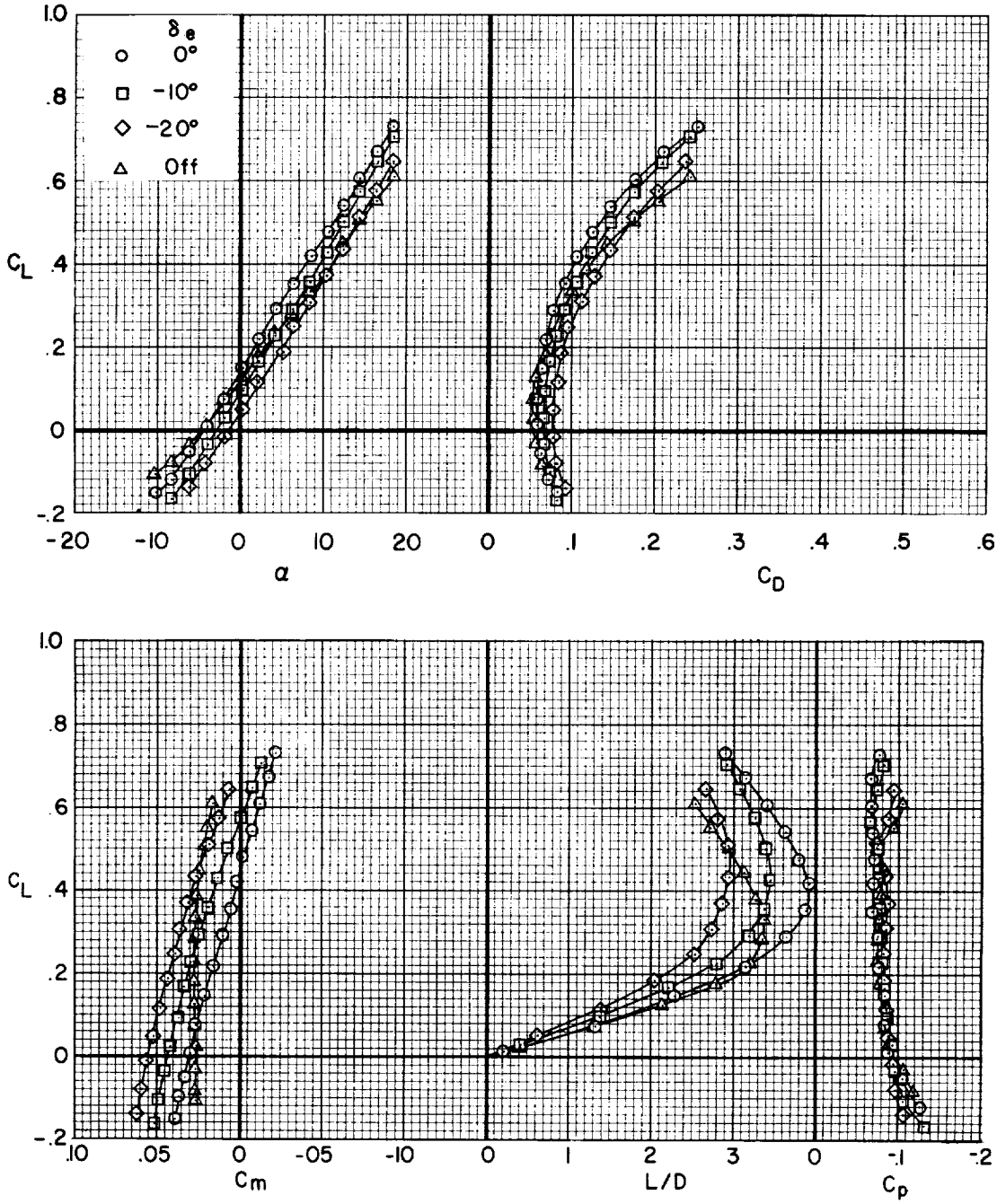

(b) $\delta_f = -10^\circ$

Figure 3.- Concluded.

A4833

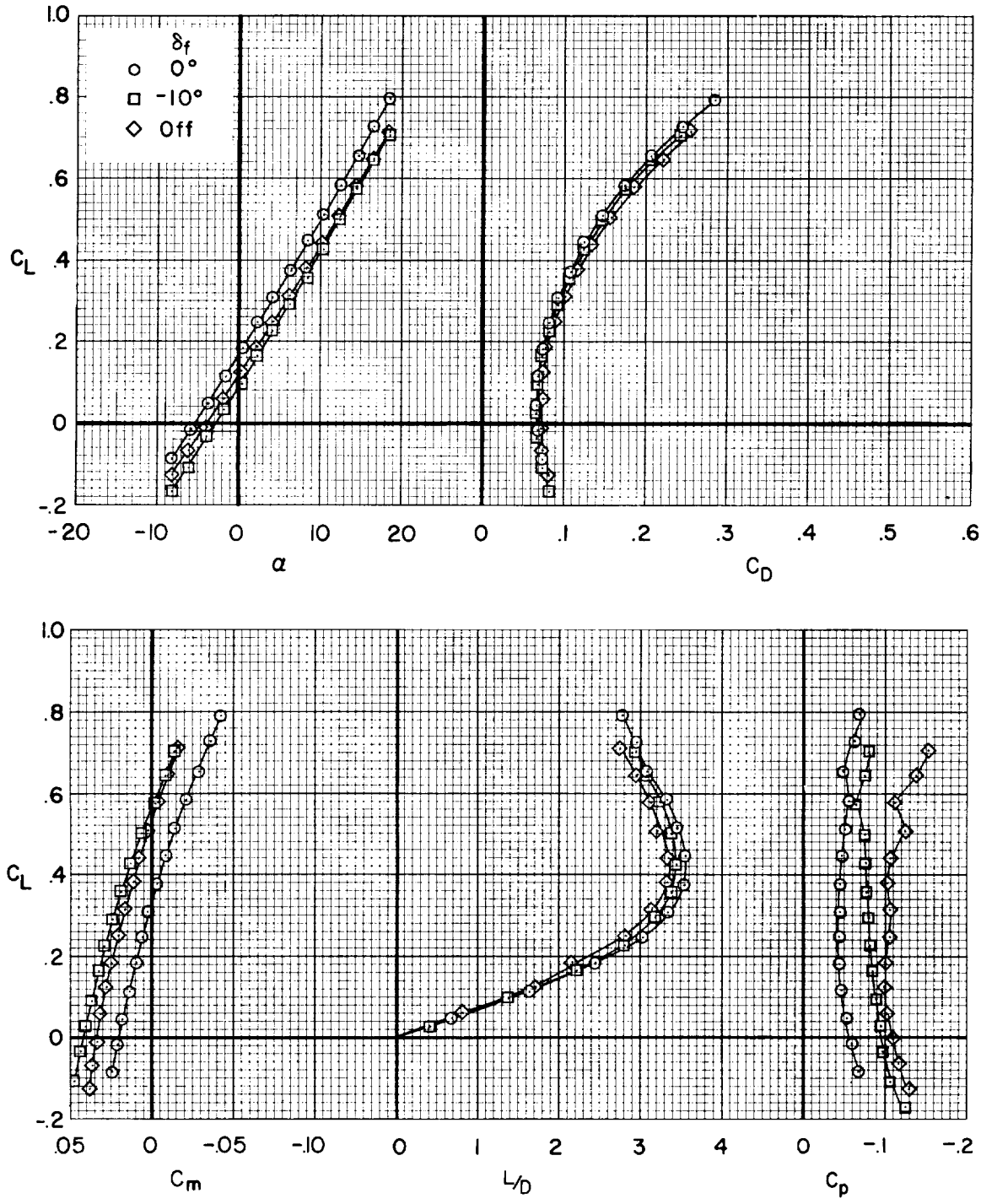

Figure 4.- The effects of trailing-edge flap deflection on the longitudinal characteristics of the model; M = 0.25, R = 15×10^6, $\delta_e = -10^\circ$, $\delta_p = 0^\circ$.

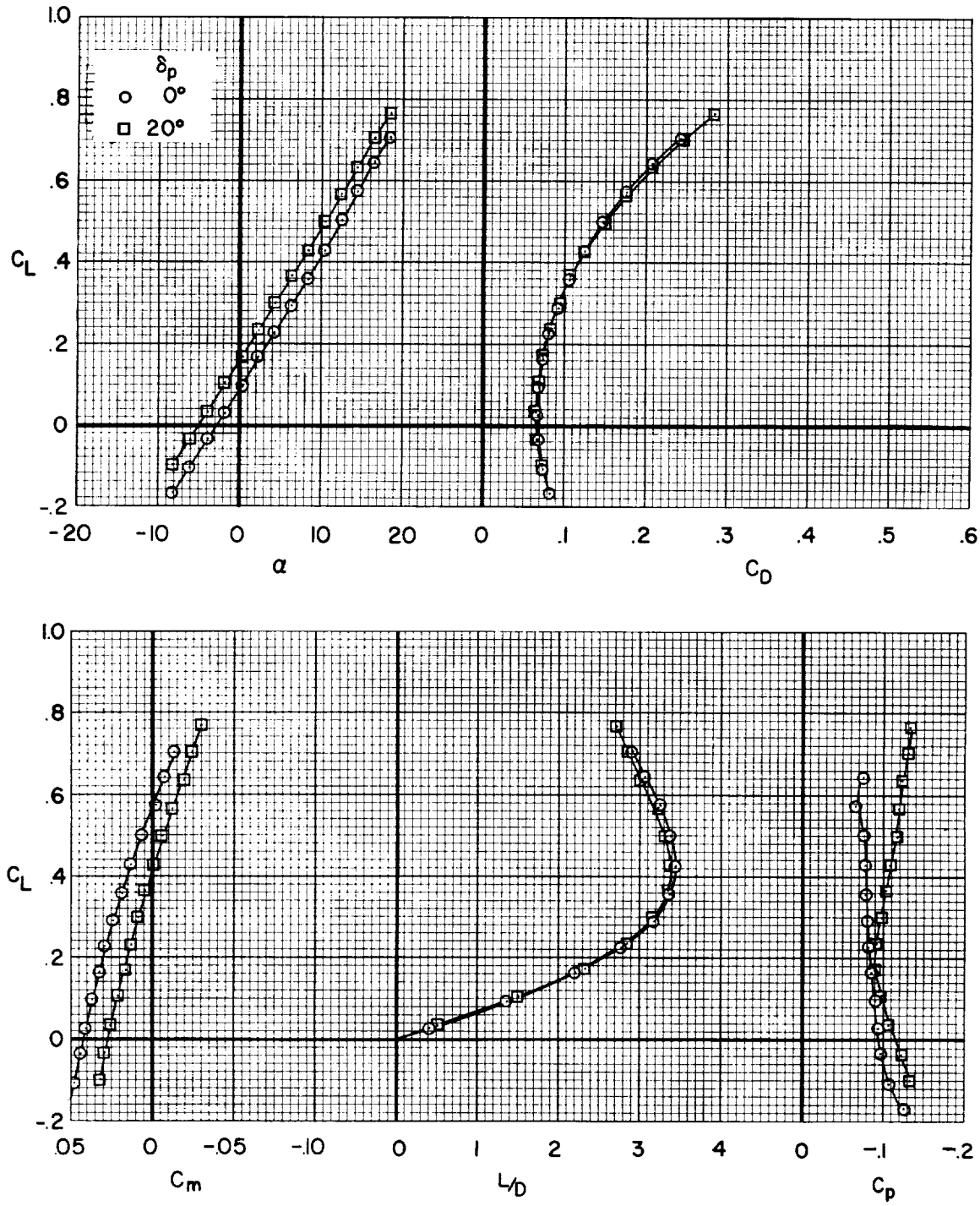

Figure 5.- The effects of pitch-flap deflection on the longitudinal characteristics of the model; M = 0.25, R = 15×10^6, δ_e = -10°, δ_f = -10°.

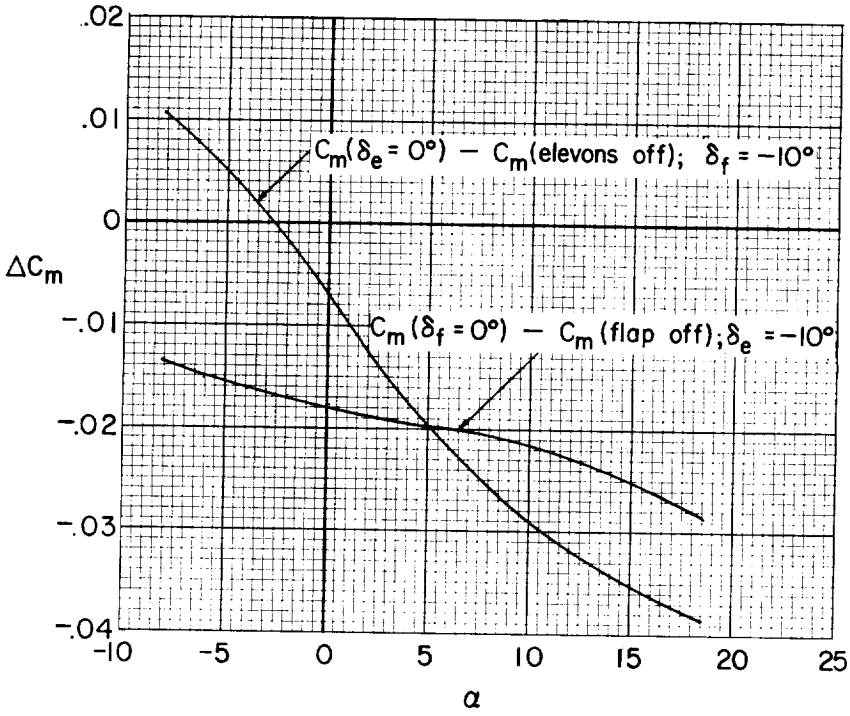

(a) Pitching-moment contributions of the elevons and of the trailing-edge flap; $\delta_p = 0^\circ$.

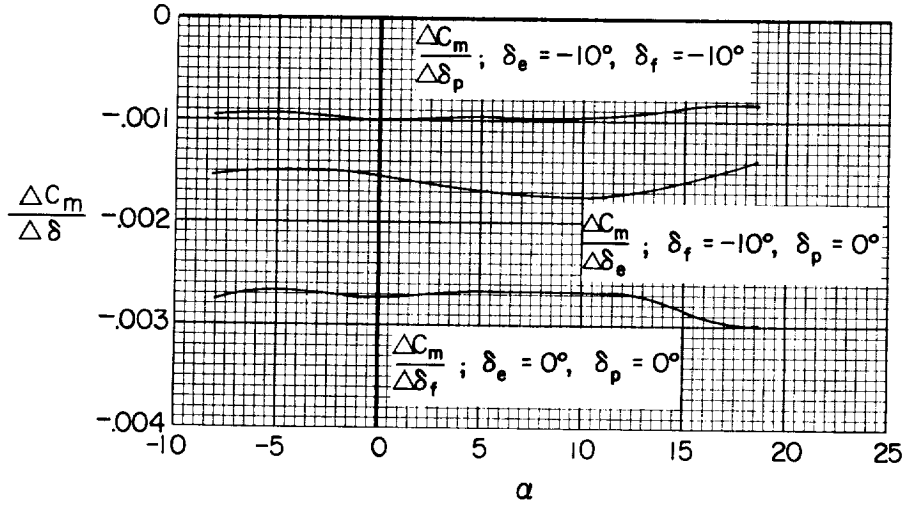

(b) Control effectiveness of the elevons, trailing-edge flap, and pitch flaps.

Figure 6.- The longitudinal control characteristics of the model; M = 0.25, R = 15×10^6.

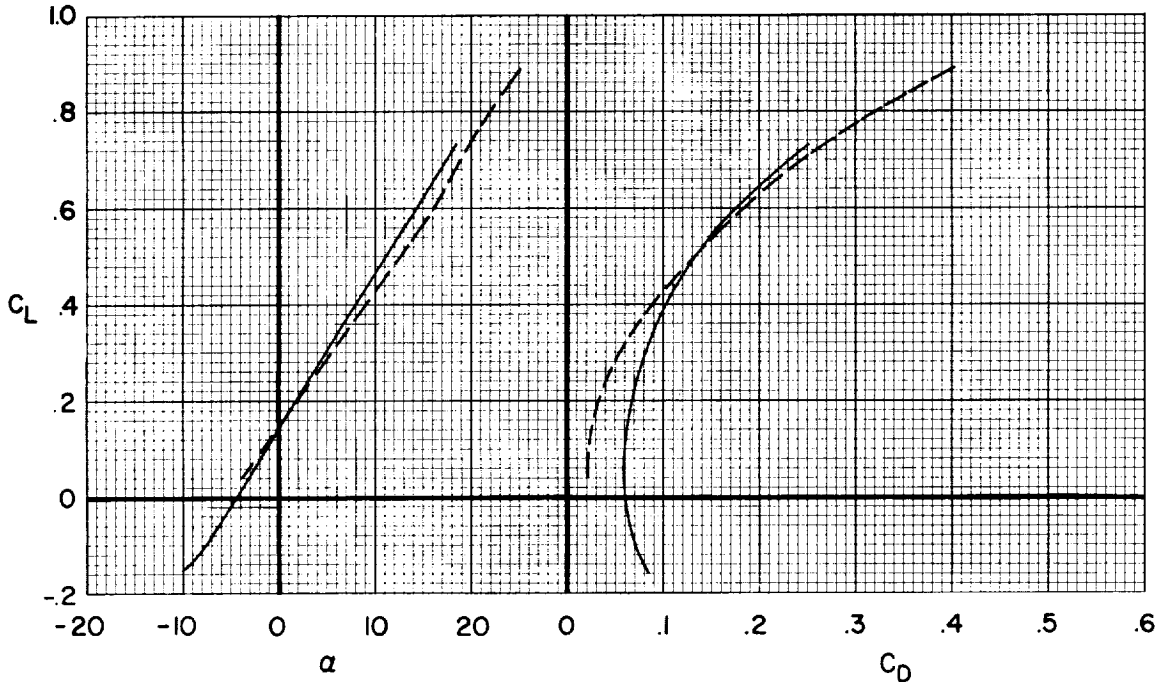

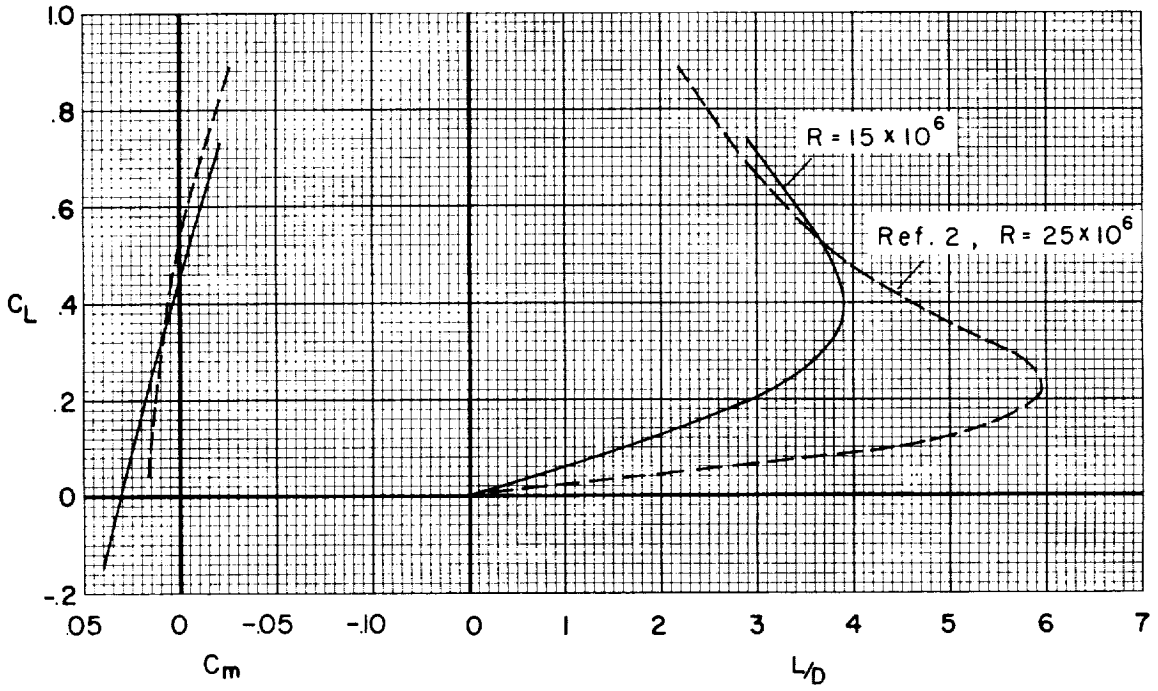

Figure 7.- A comparison of the longitudinal characteristics of the model with those of the configuration of reference 2; M = 0.25, $\delta_e = 0^\circ$, $\delta_f = -10^\circ$, $\delta_p = 0^\circ$.

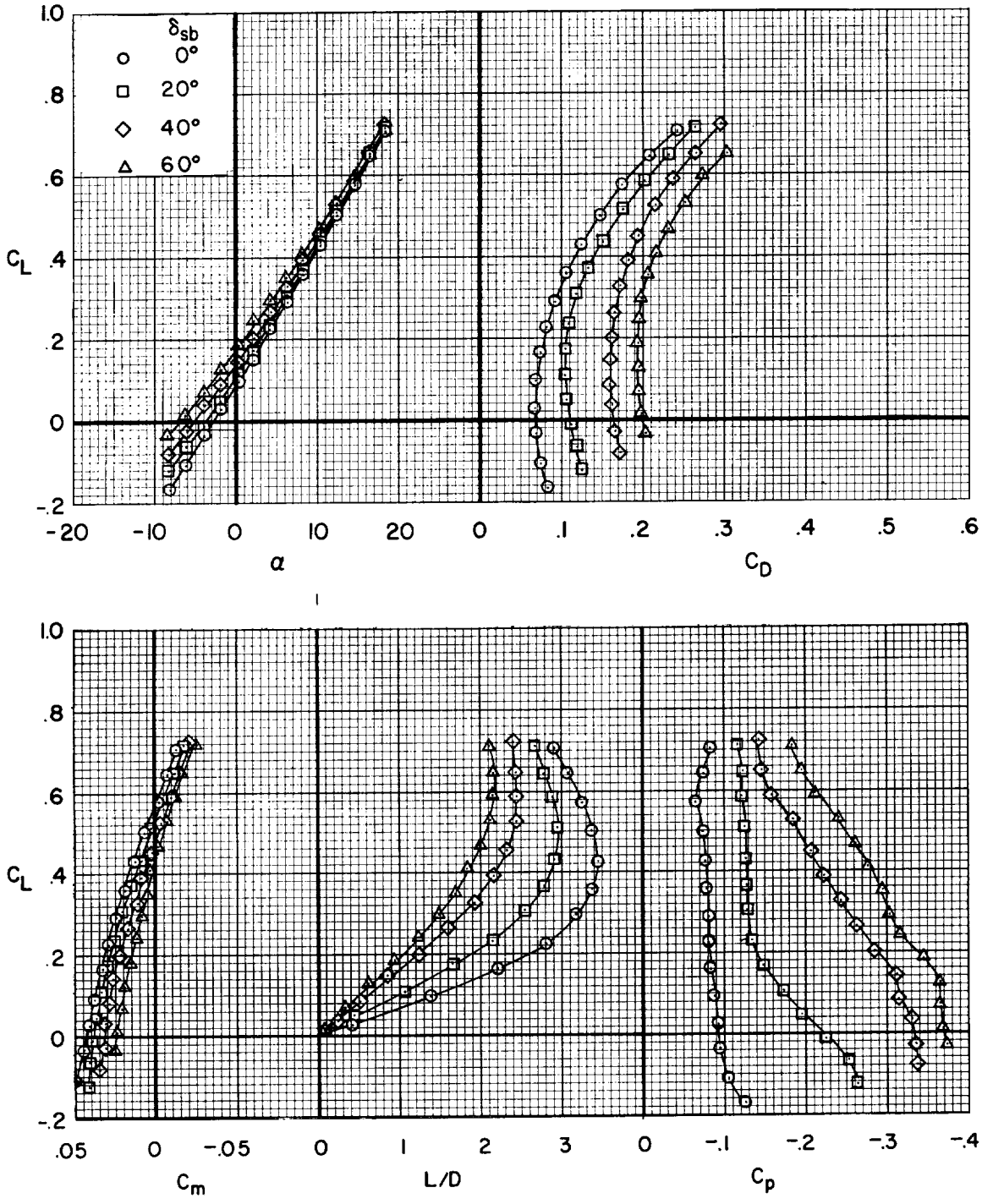

Figure 8.- The effects of speed-brake deflection on the longitudinal characteristics of the model; M = 0.25, R = 15×10⁶, δ_e = -10°, δ_f = -10°, δ_p = 0°.

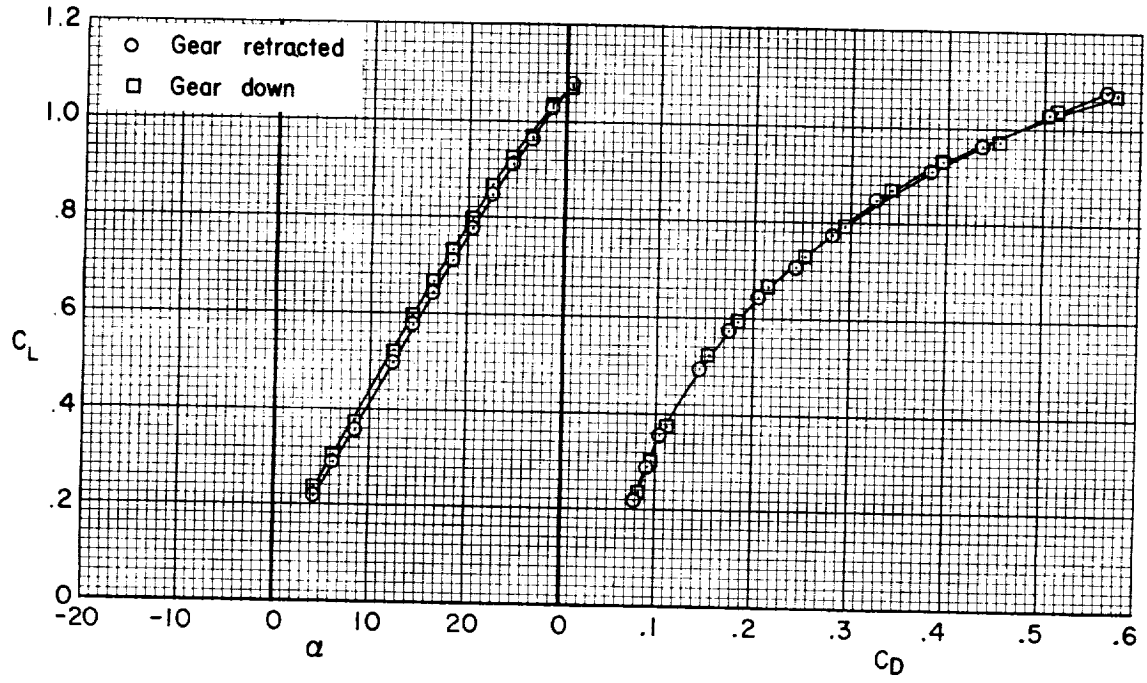

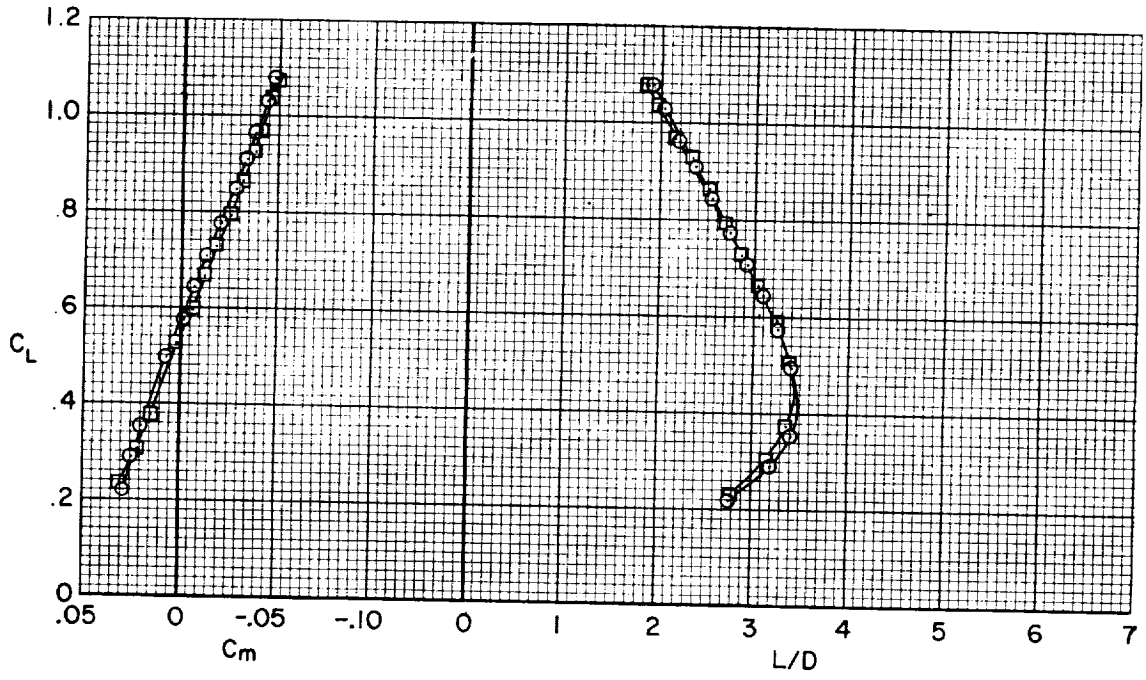

Figure 9.- The effects of landing-gear extension on the longitudinal characteristics of the model; M = 0.25, R = 15×10^6, δ_e = -10°, δ_f = -10°, δ_p = 0°.

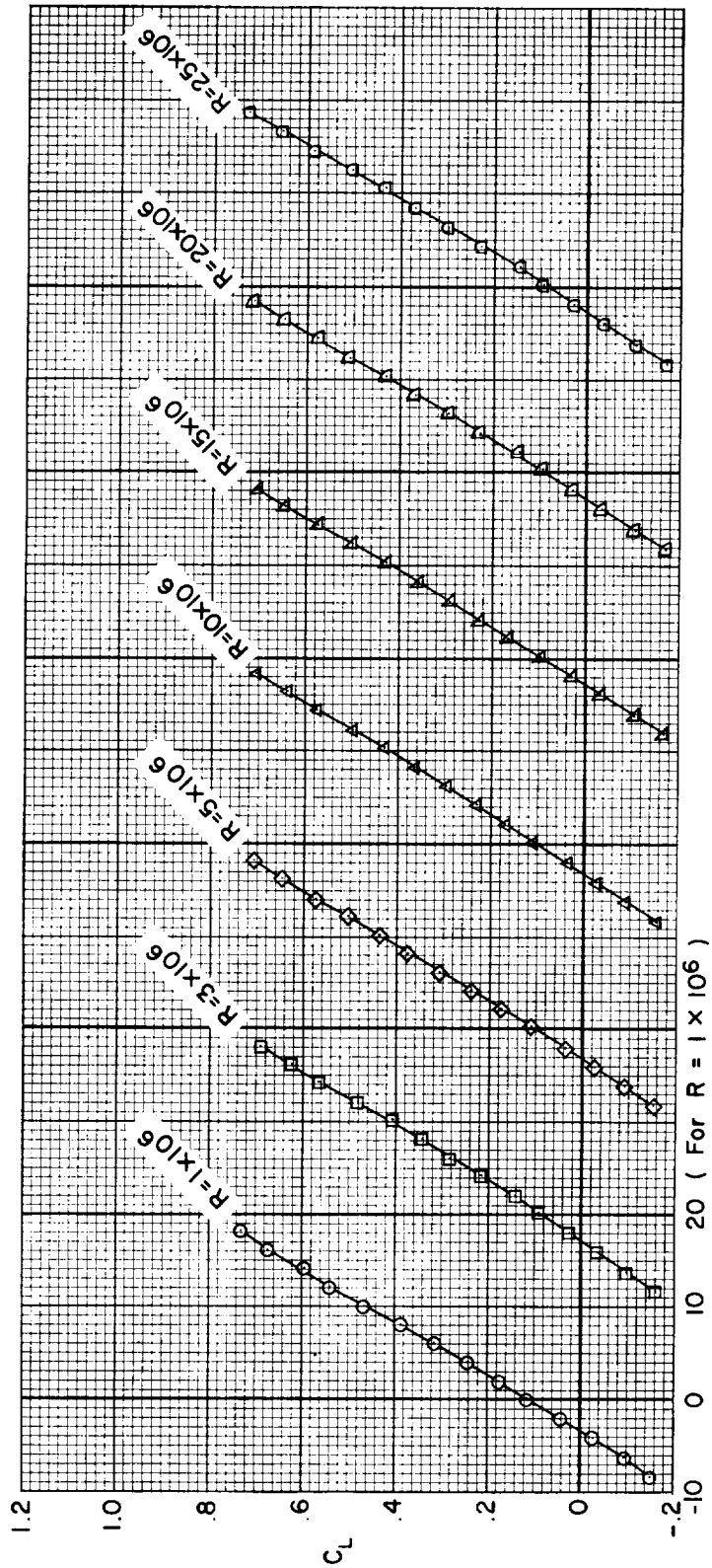

(a) Lift coefficient.

Figure 10.- The longitudinal characteristics of the model at several Reynolds numbers; M = 0.25, $\delta_e = -10^\circ$, $\delta_f = -10^\circ$, $\delta_p = 0^\circ$.

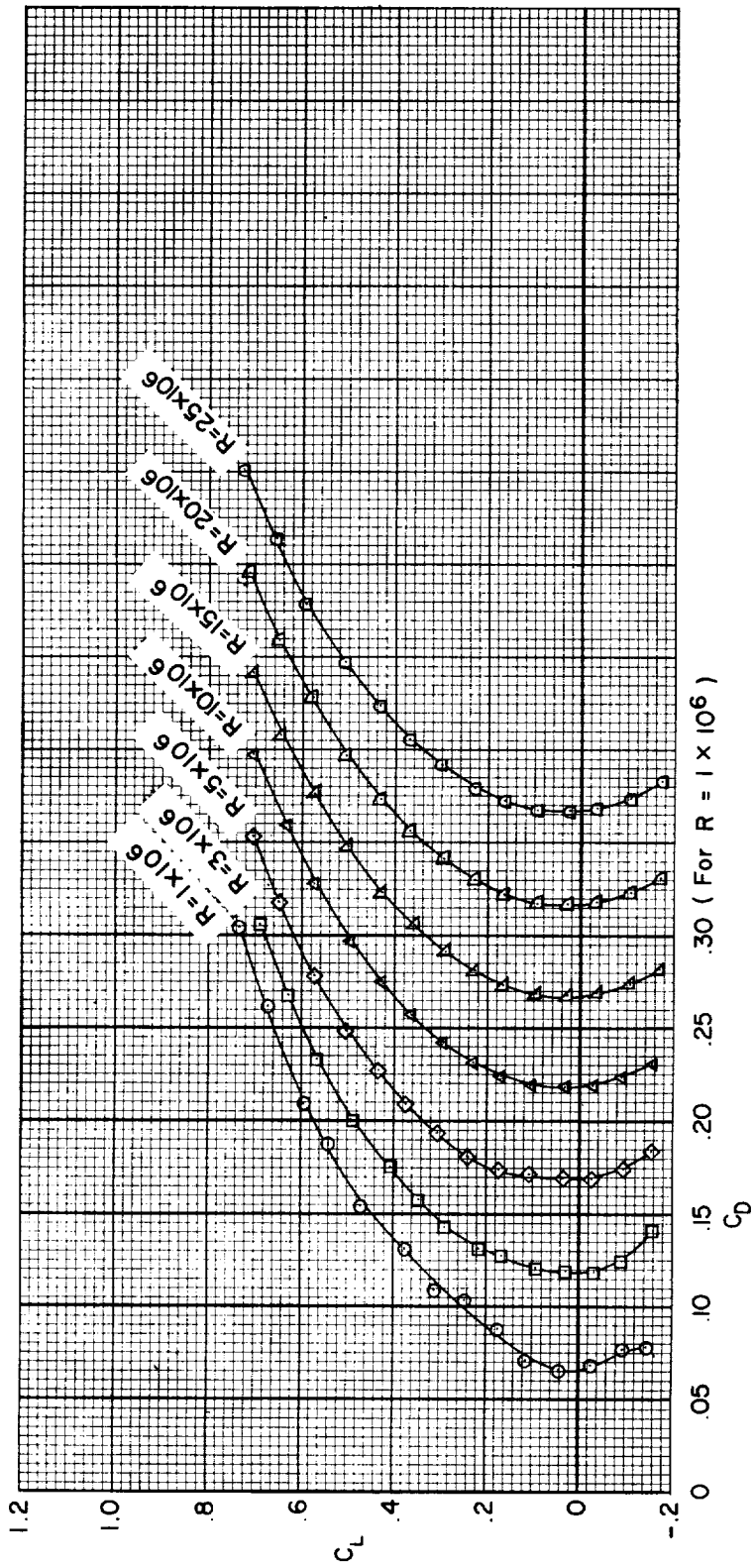

(b) Drag coefficient.

Figure 10.- Continued.

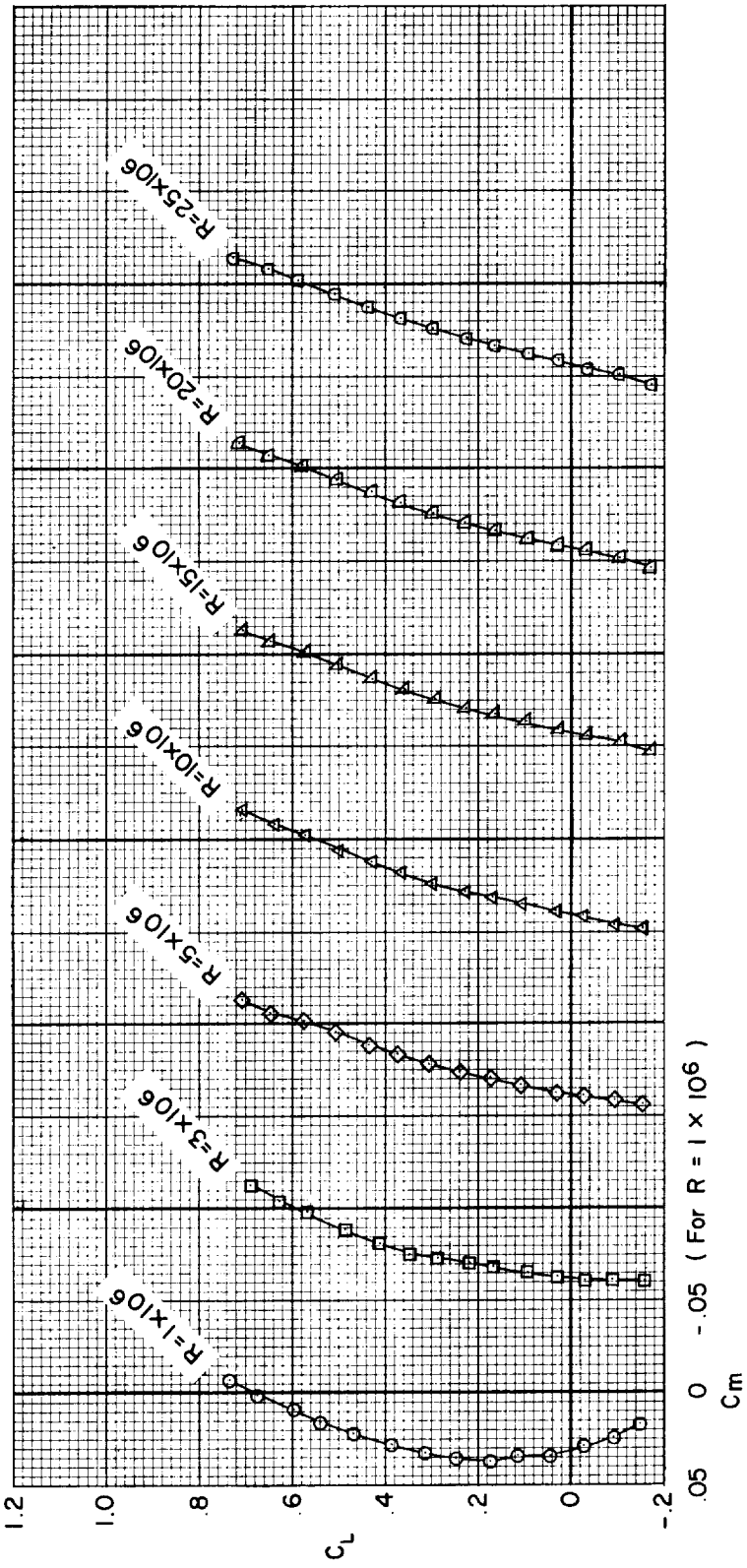

(c) Pitching-moment coefficient.

Figure 10.- Continued.

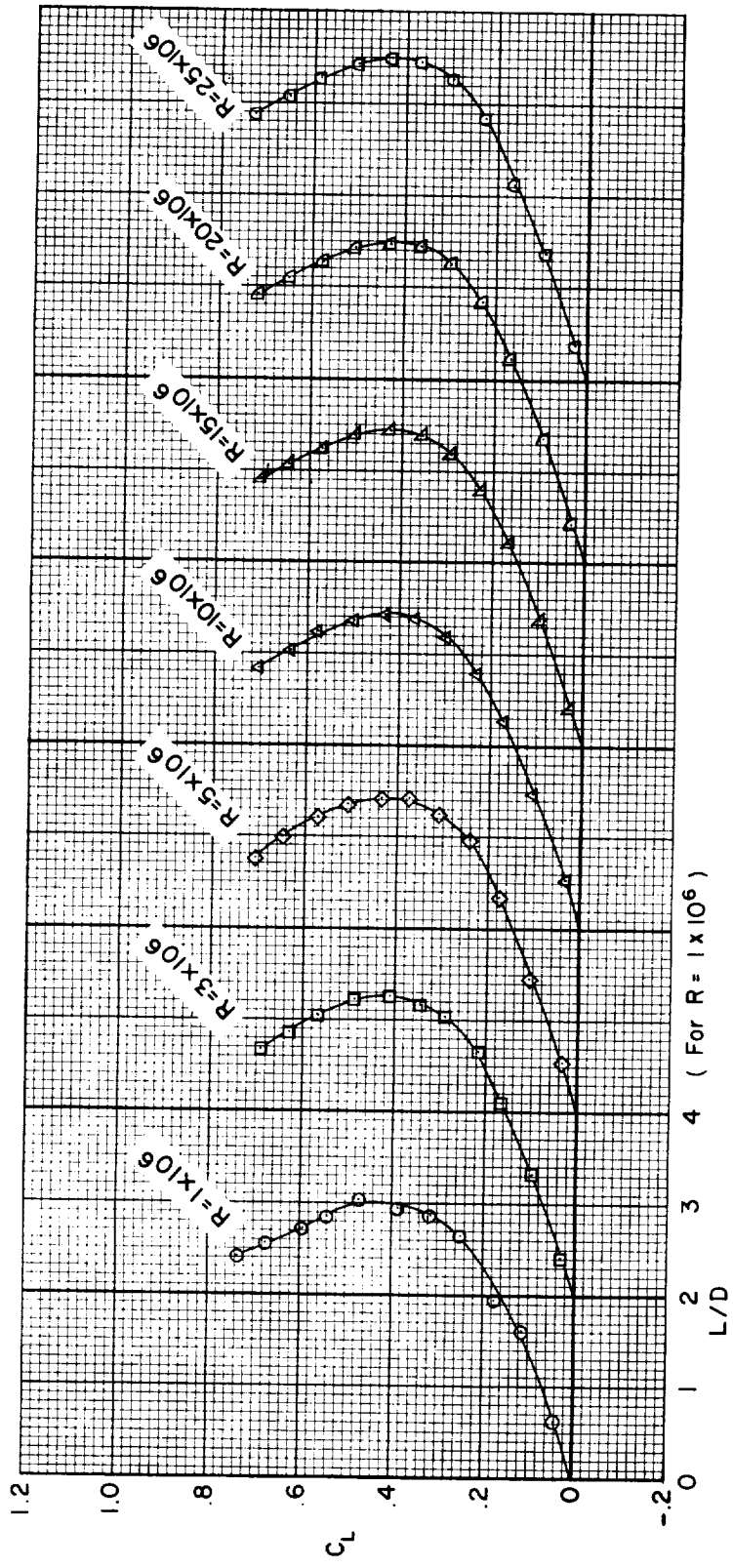

(d) Lift-drag ratio.

Figure 10.- Continued.

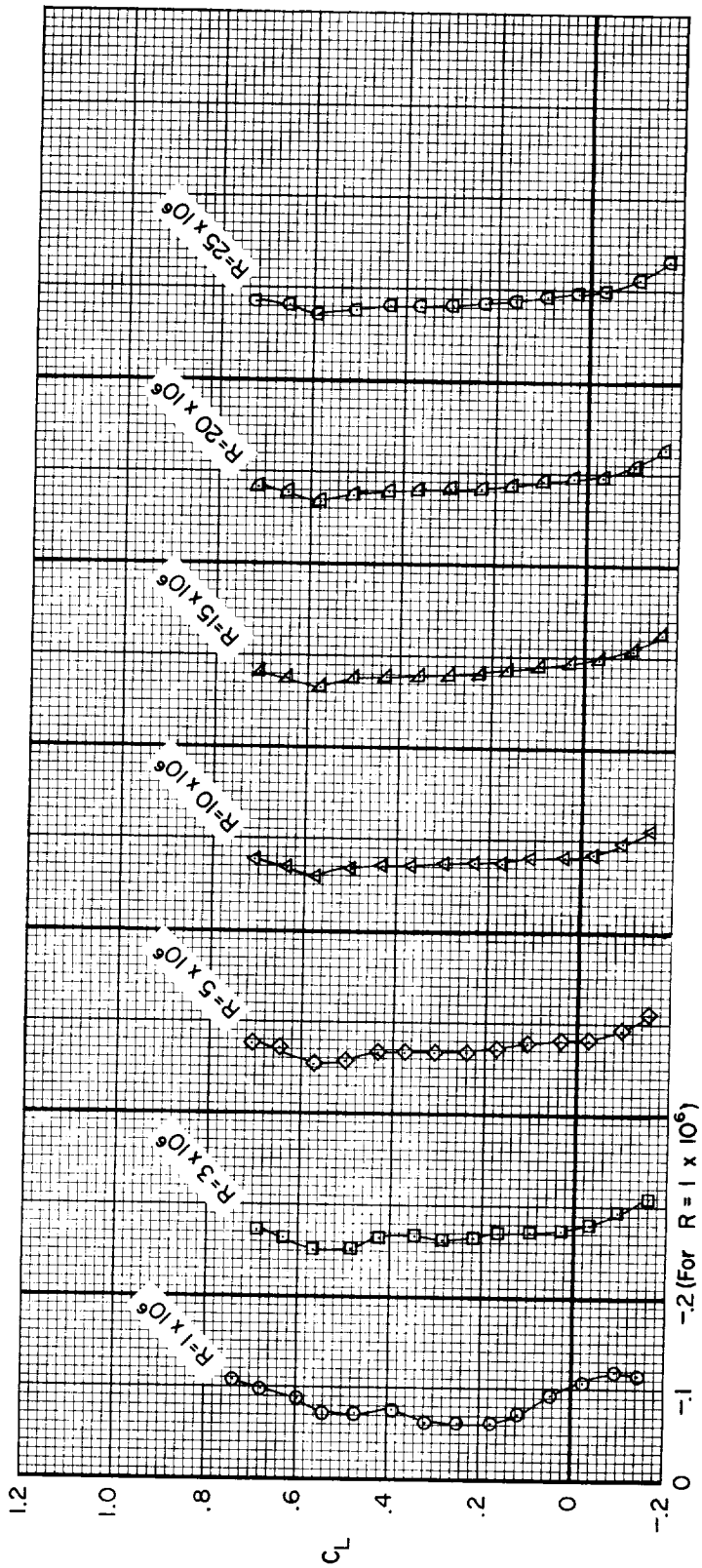

(e) Base-pressure coefficient.

Figure 10.- Concluded.

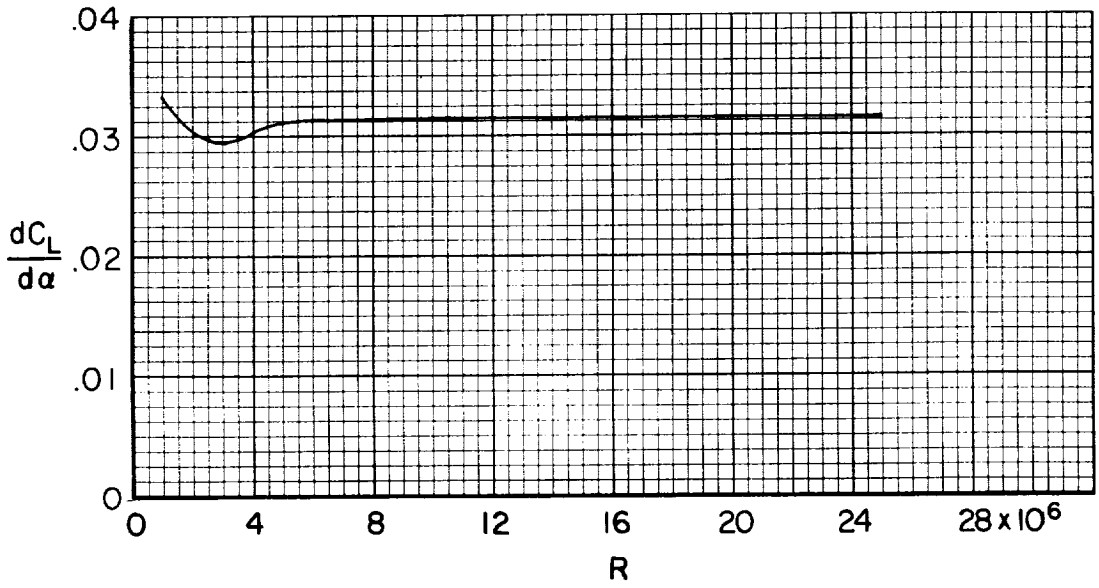

(a) Lift-curve slope, $C_L = 0$.

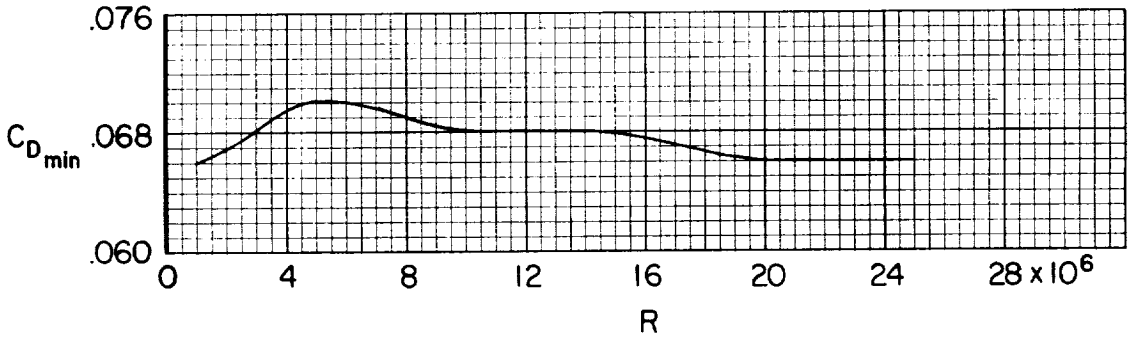

(b) Minimum drag coefficient.

Figure 11.- The effects of Reynolds number on the lift-curve slope, minimum drag, pitching-moment-curve slope, and lift-drag ratio; $M = 0.25$, $\delta_e = -10^\circ$, $\delta_f = -10^\circ$, $\delta_p = 0^\circ$.

A 4 8 3

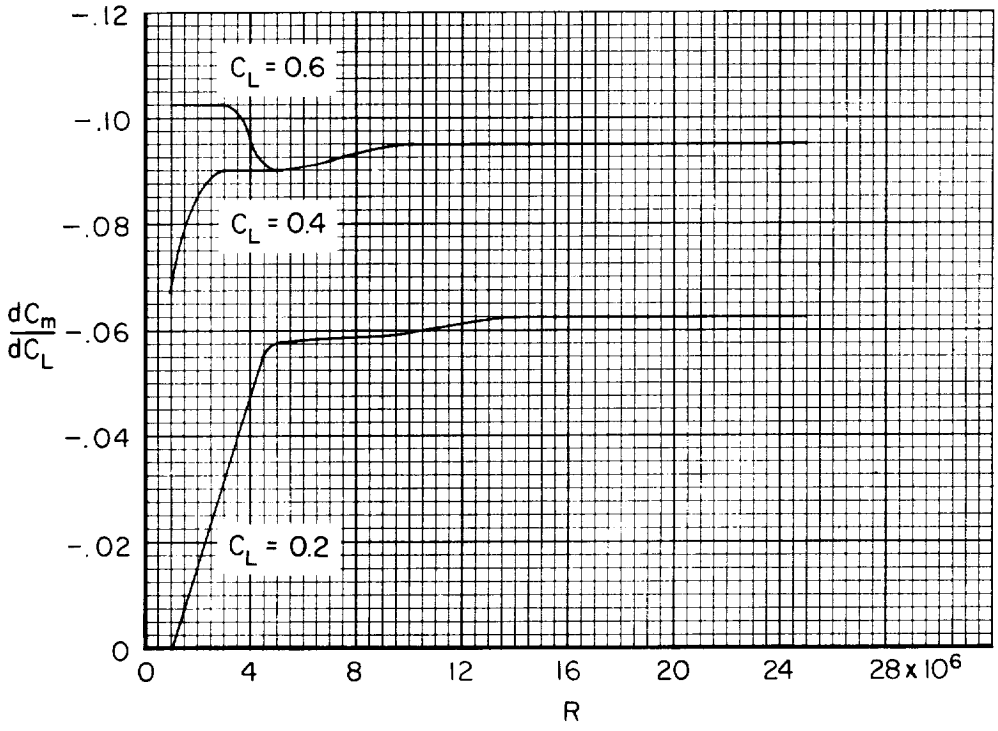

(c) Pitching-moment-curve slope.

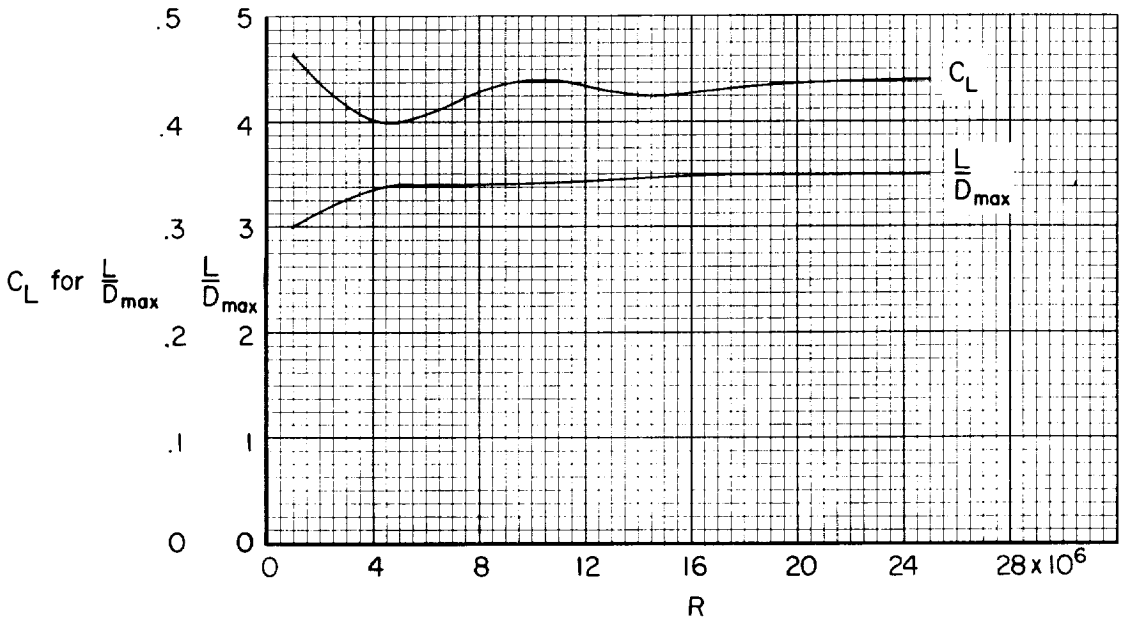

(d) Lift-drag ratio.

Figure 11.- Concluded.

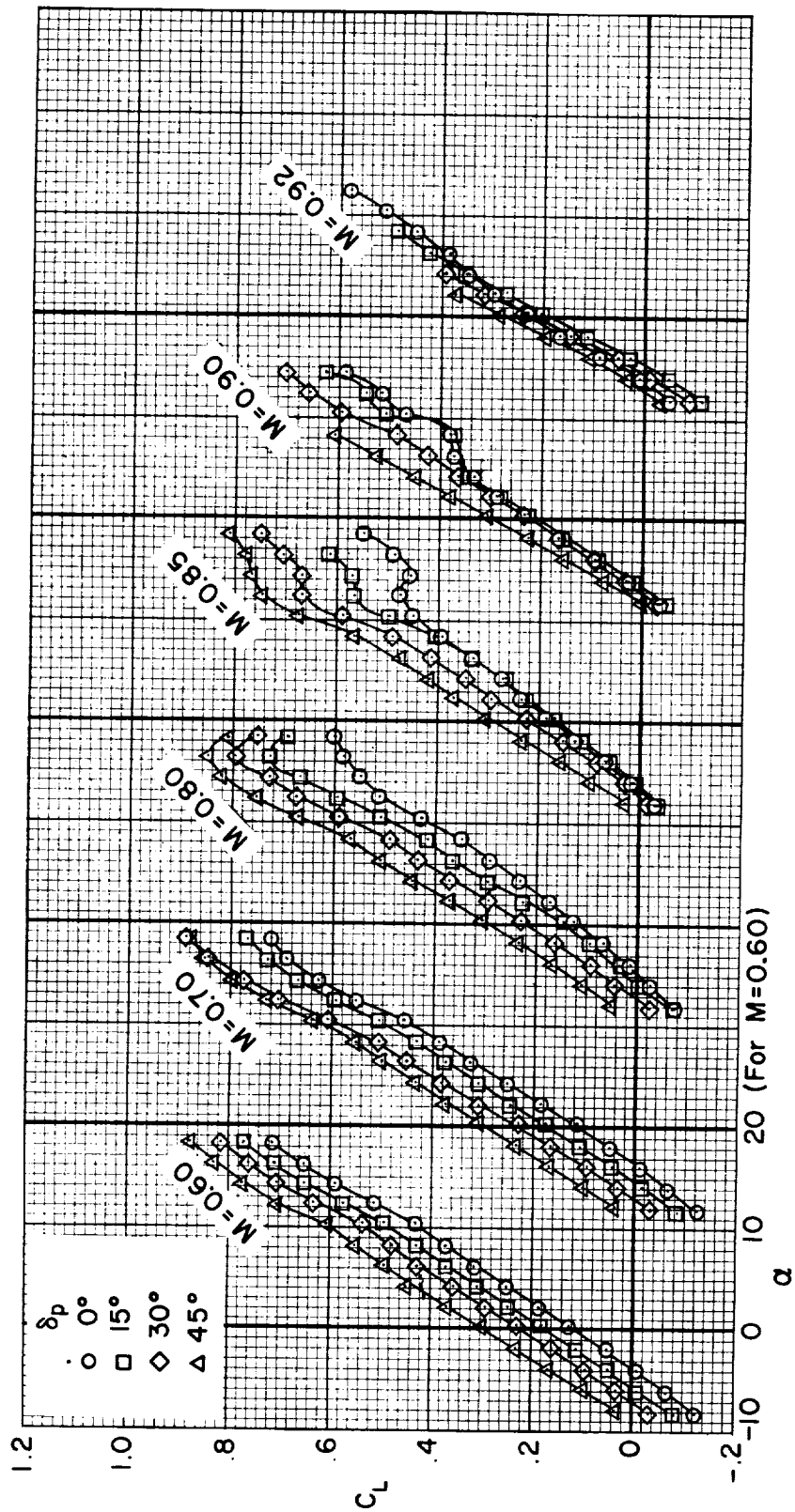

(a) Lift coefficient.

Figure 12.- The effects of pitch-flap deflection on the longitudinal characteristics of the model, elevons at -10°, for several Mach numbers; R = 5×10⁶.

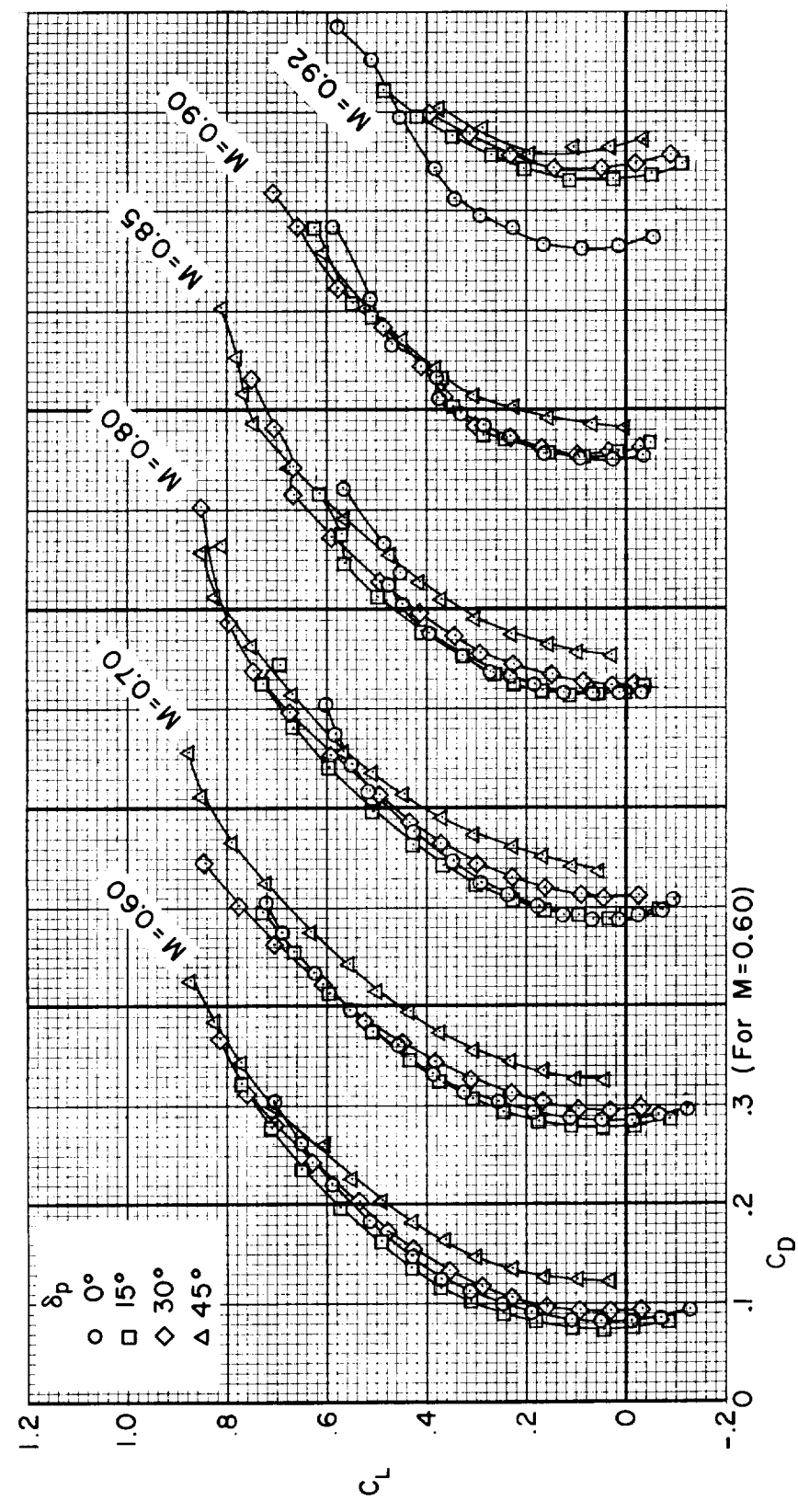

(b) Drag coefficient.

Figure 12.- Continued.

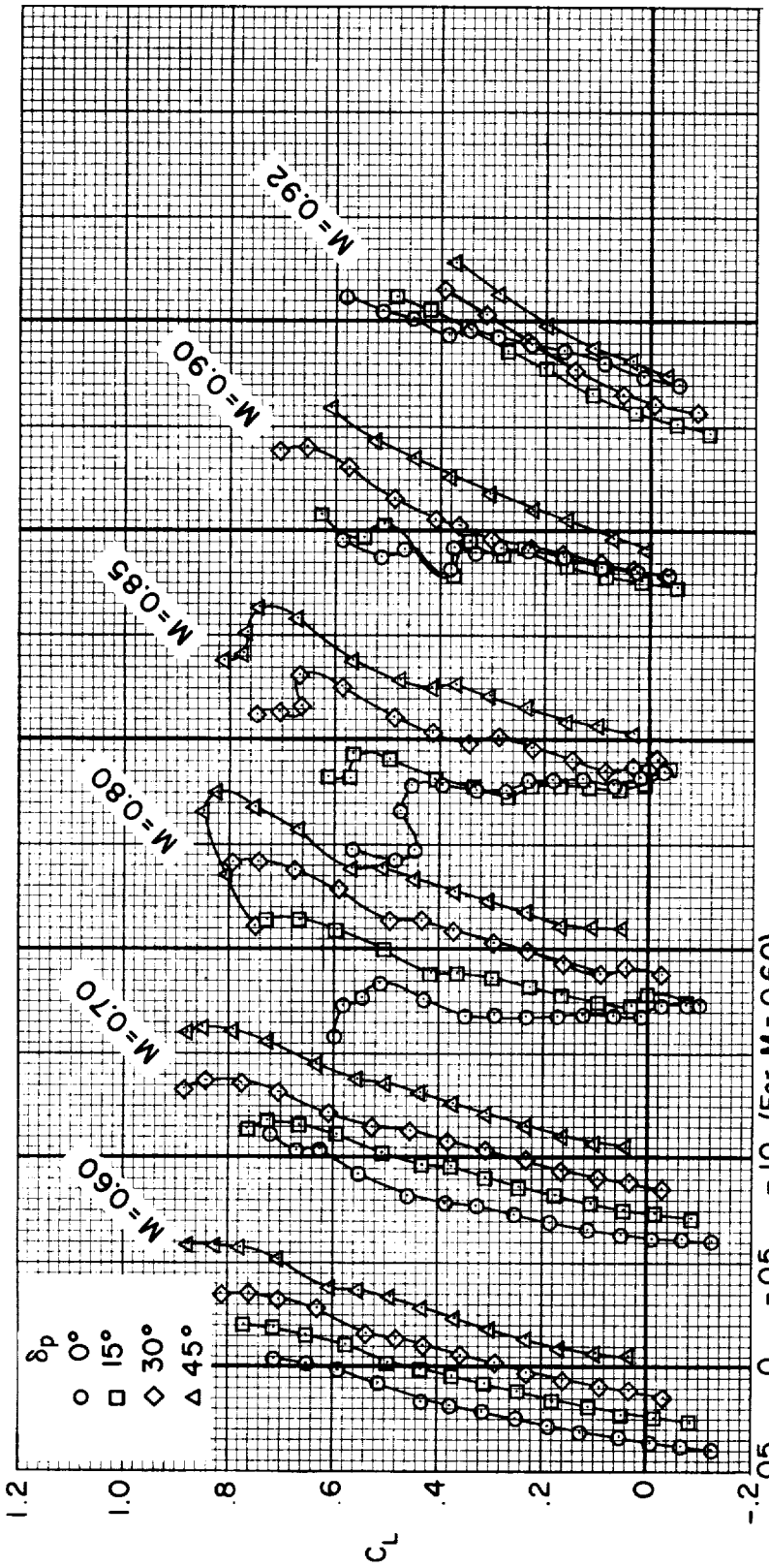

(c) Pitching-moment coefficient.

Figure 12.- Continued.

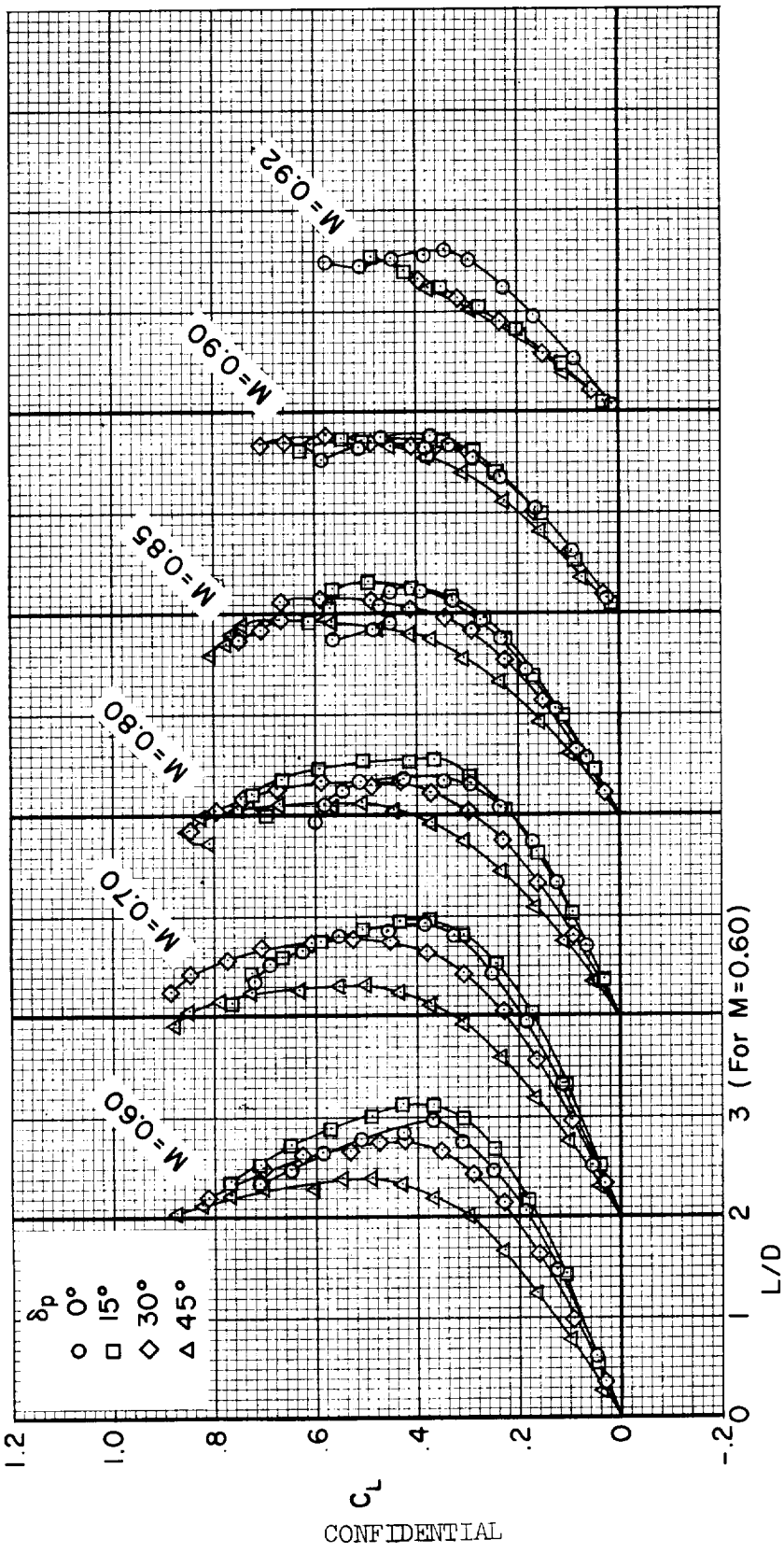

(d) Lift-drag ratio.

Figure 12.- Continued.

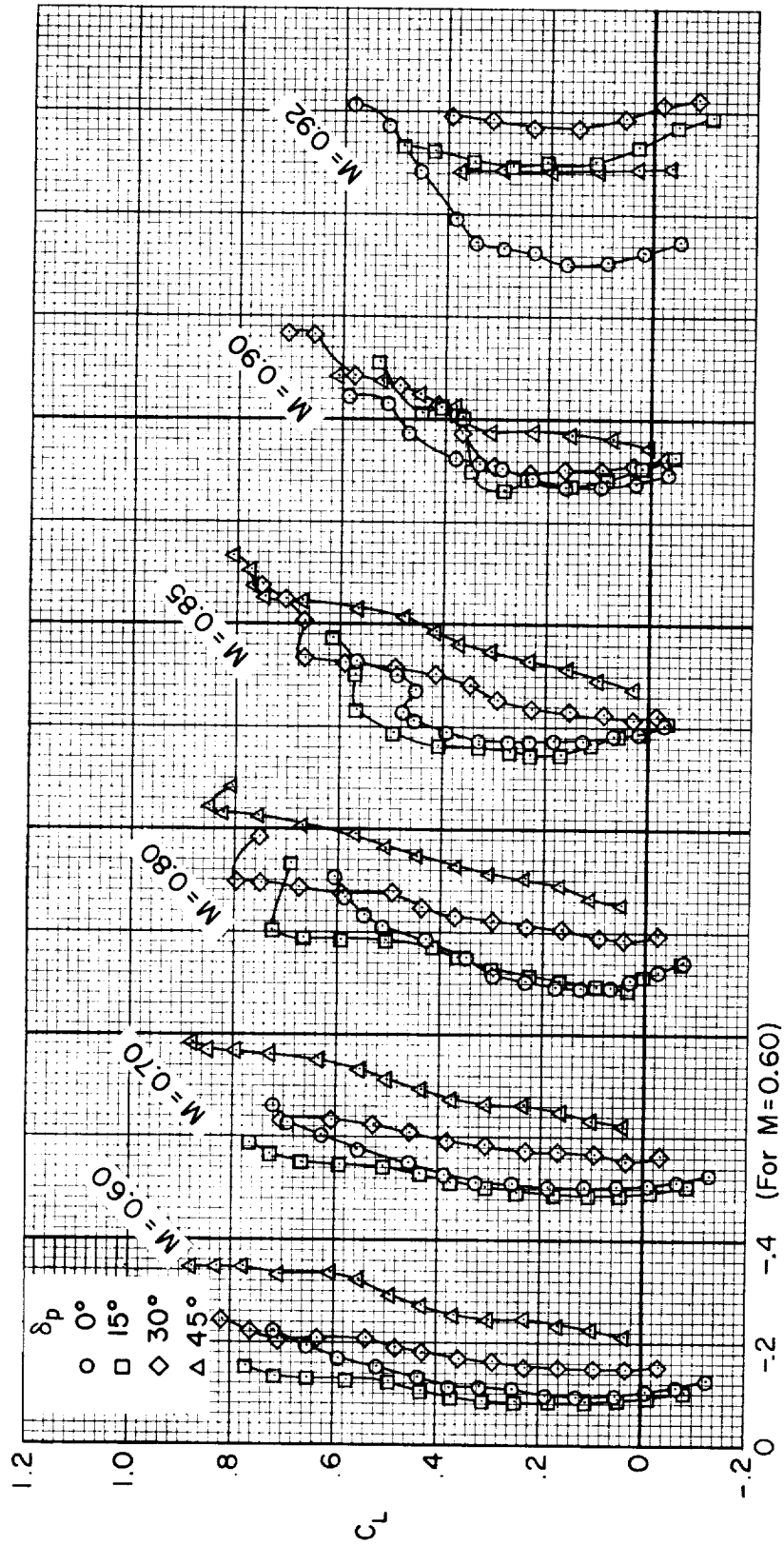

(e) Base-pressure coefficient.

Figure 12.- Concluded.

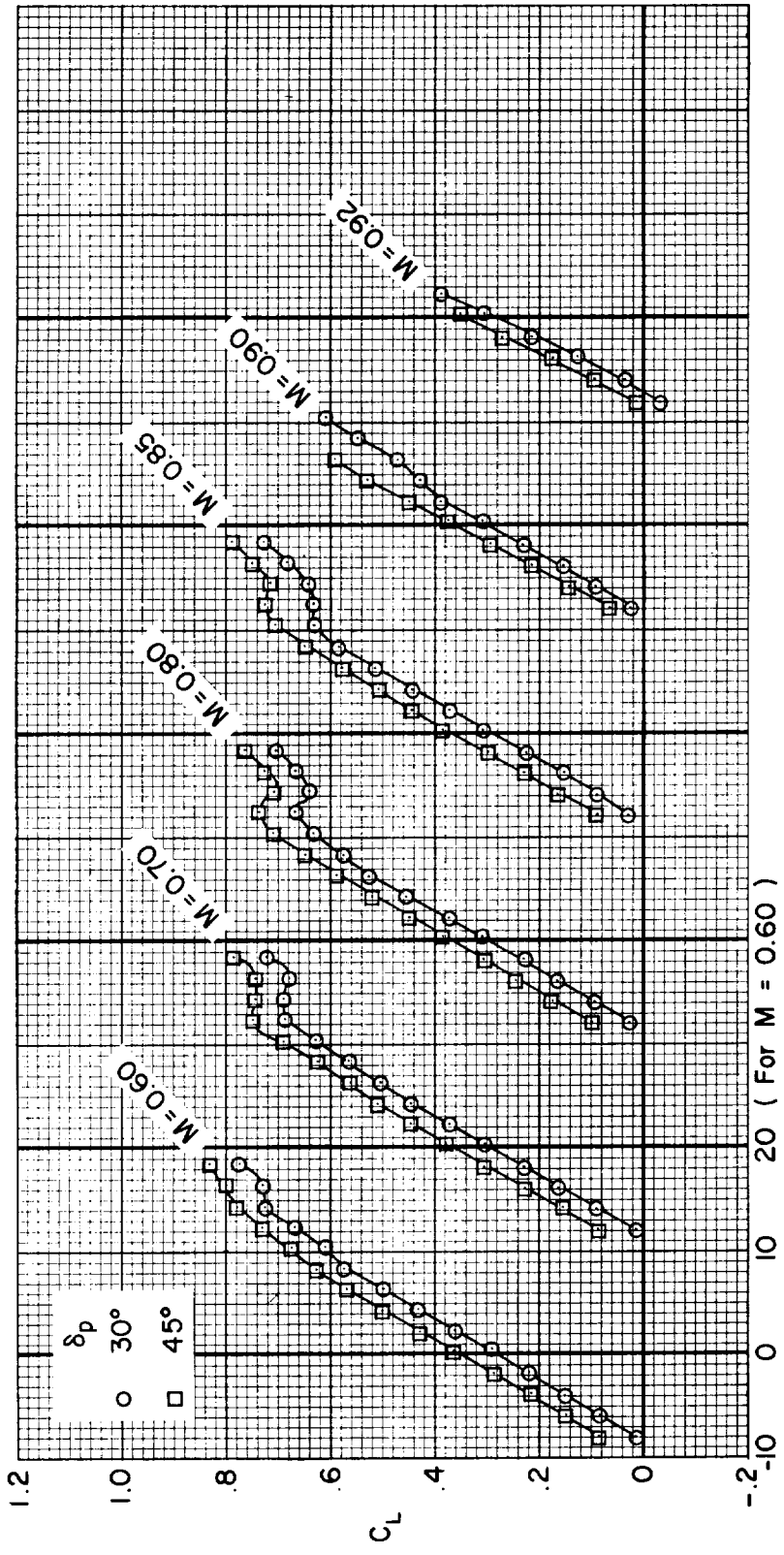

(a) Lift coefficient.

Figure 13.- The effects of pitch-flap deflection on the longitudinal characteristics of the model, elevons at 0°, for several Mach numbers; R = 5×10^{6}.

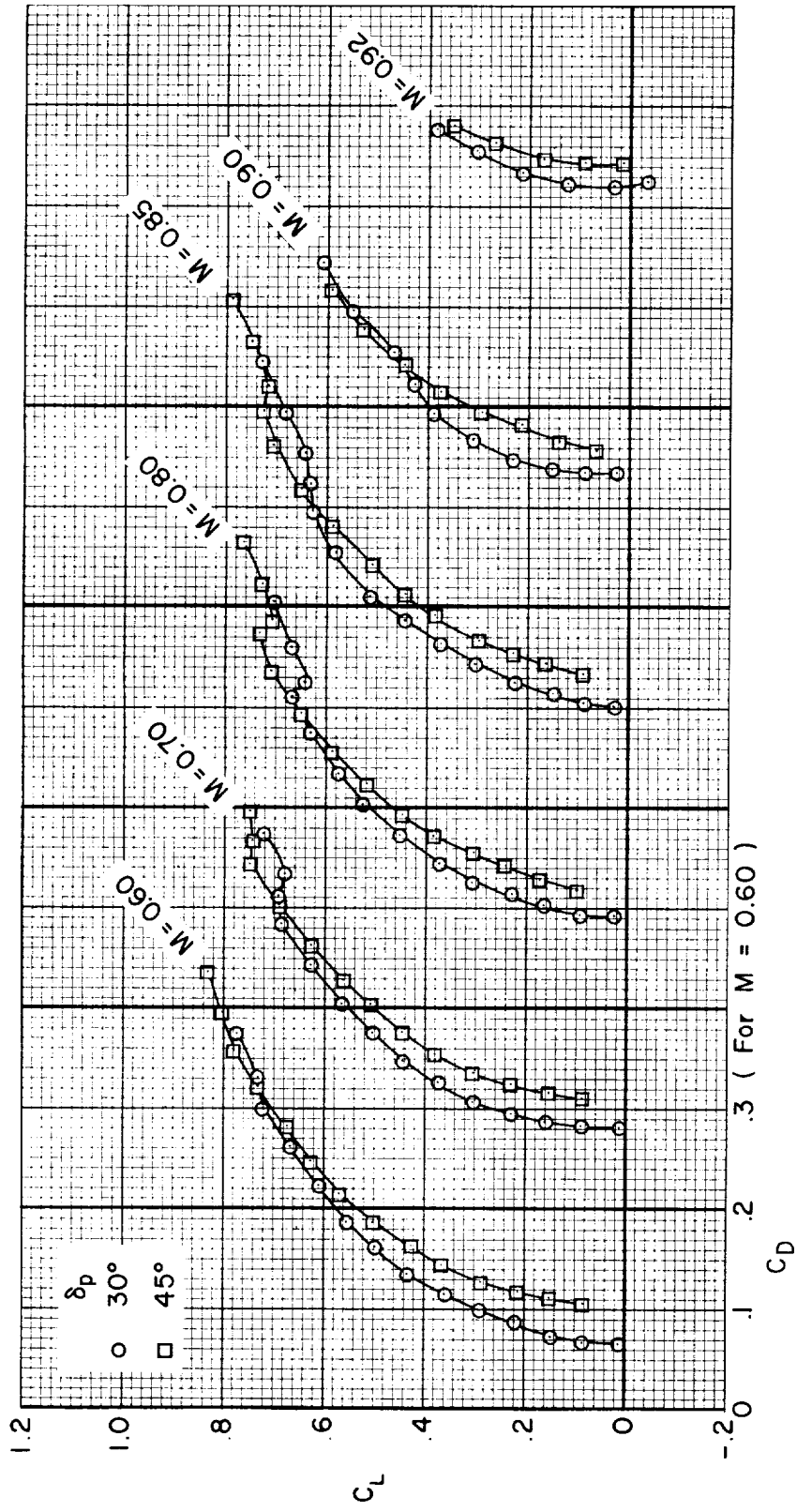

(b) Drag coefficient.

Figure 13.- Continued.

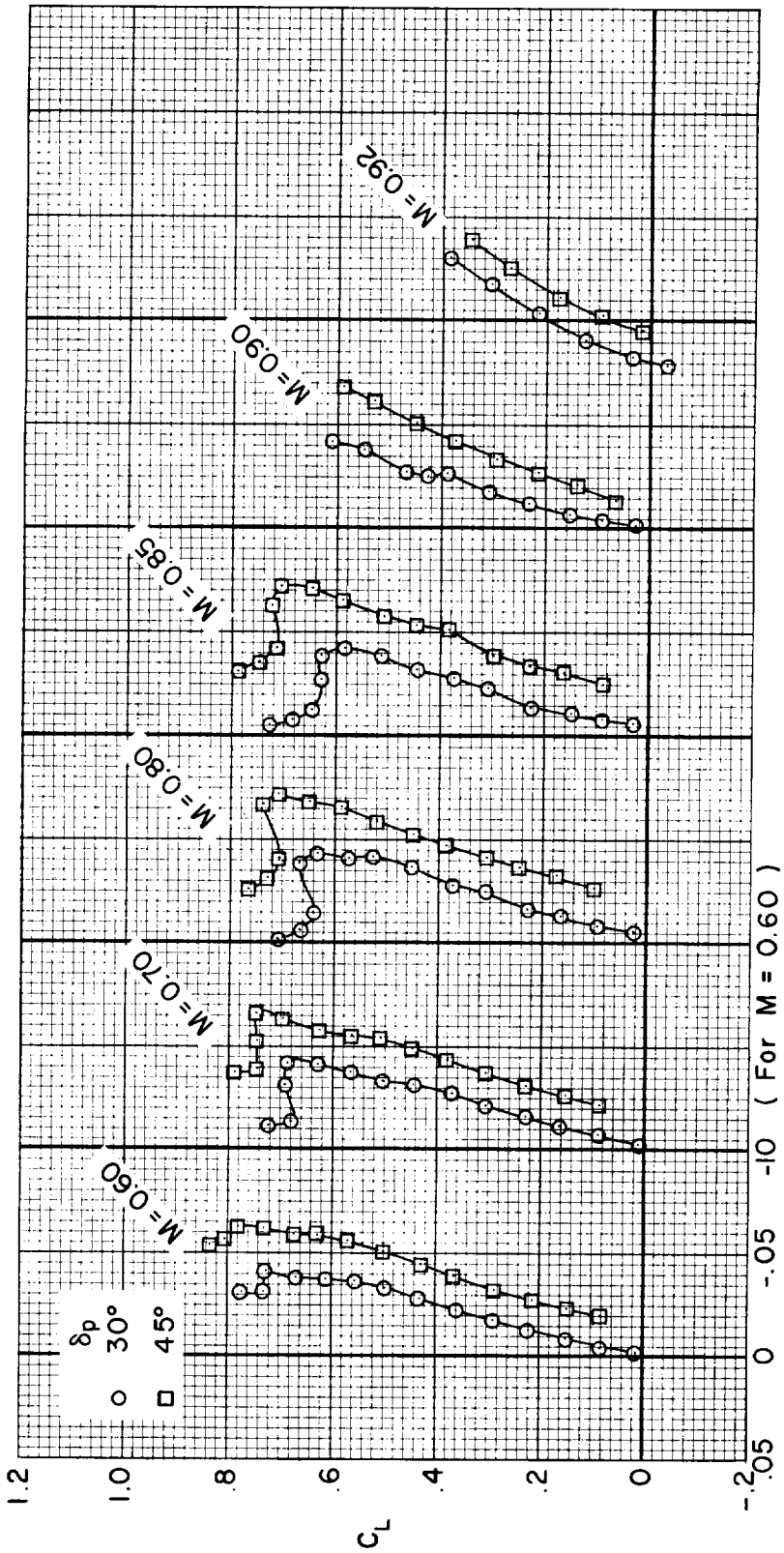

(c) Pitching-moment coefficient.

Figure 13.- Continued.

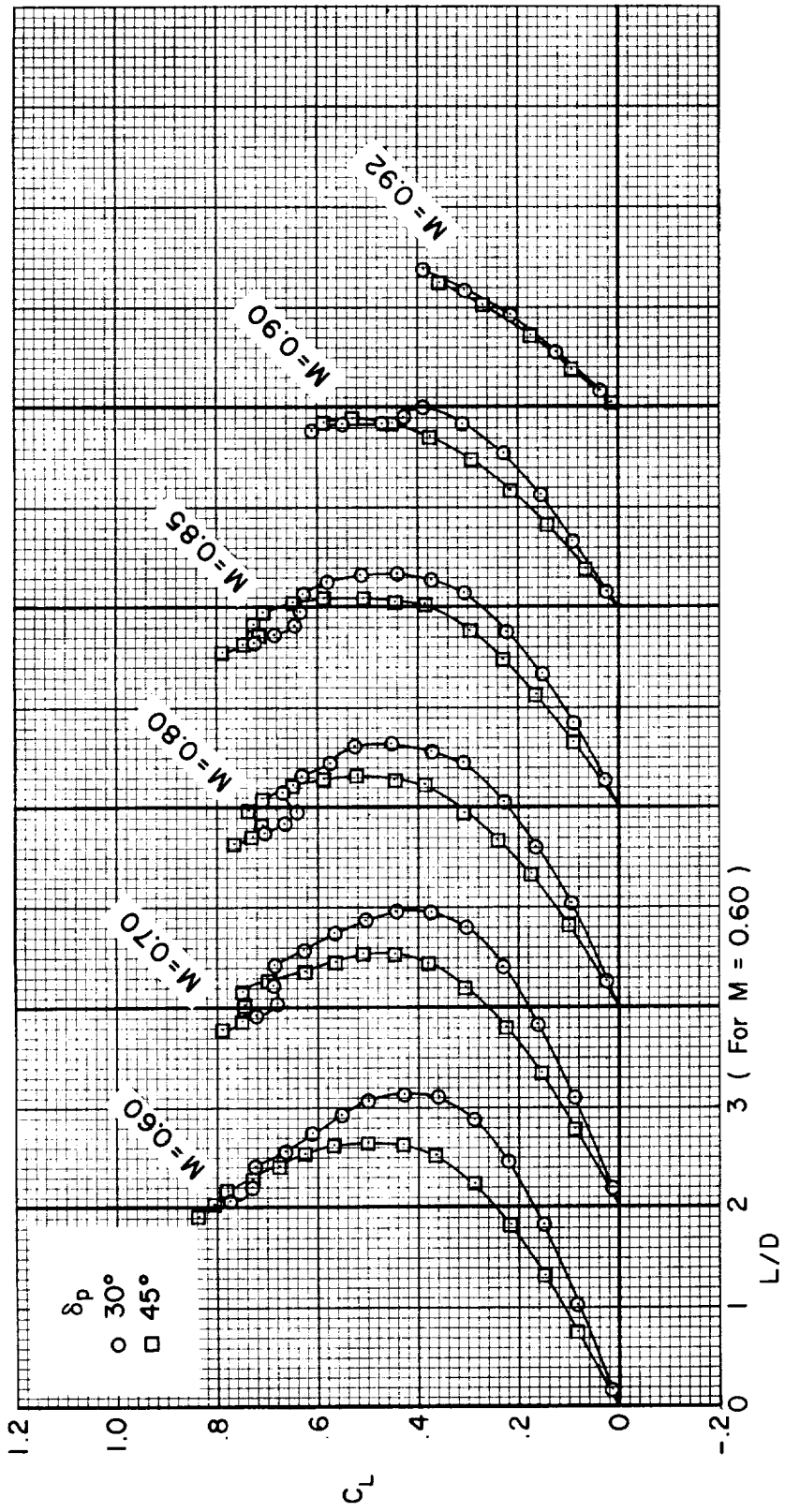

(d) Lift-drag ratio.

Figure 13.- Continued.

A
F
8
3

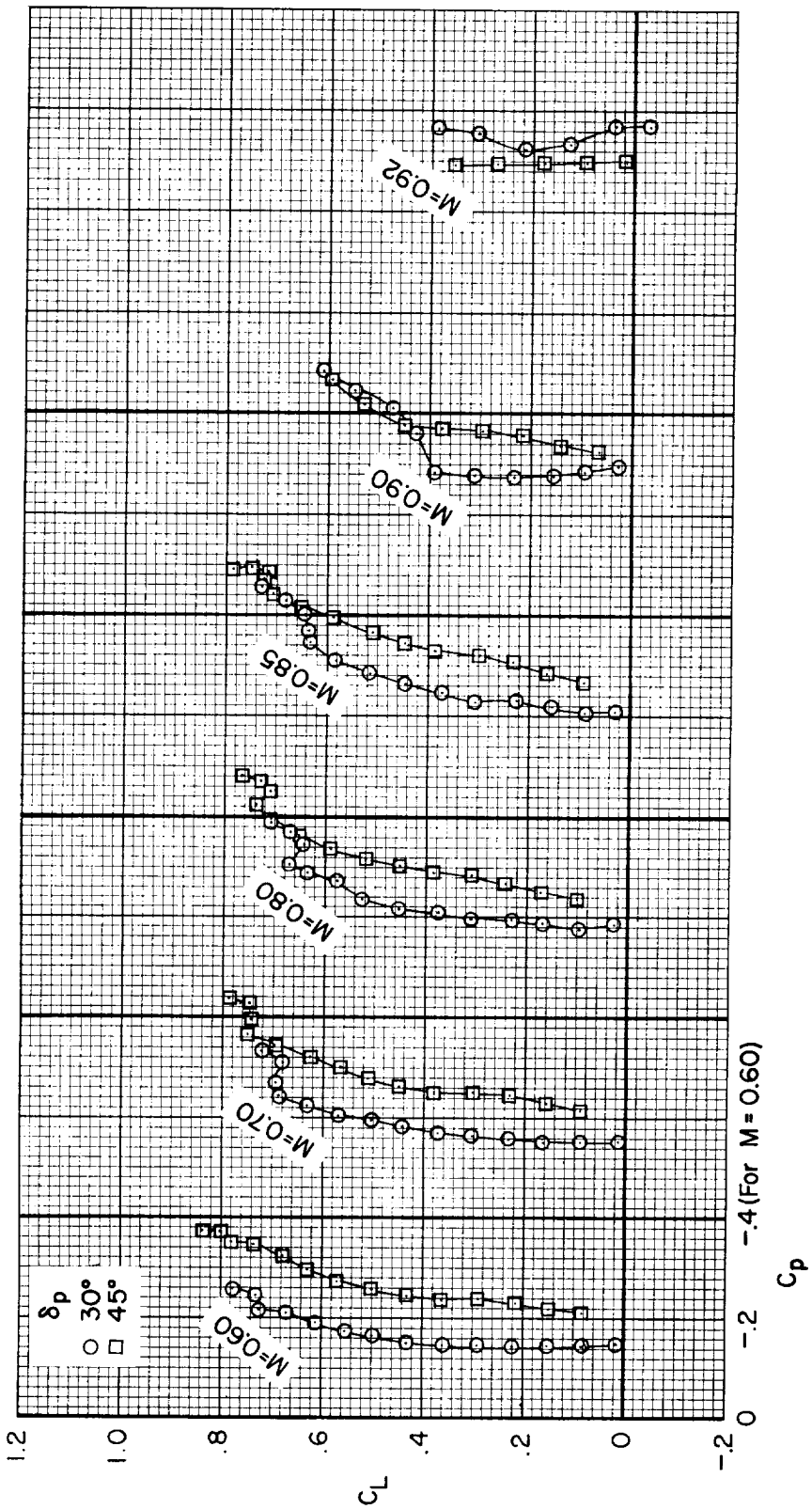

(e) Base-pressure coefficient.

Figure 13.- Concluded.

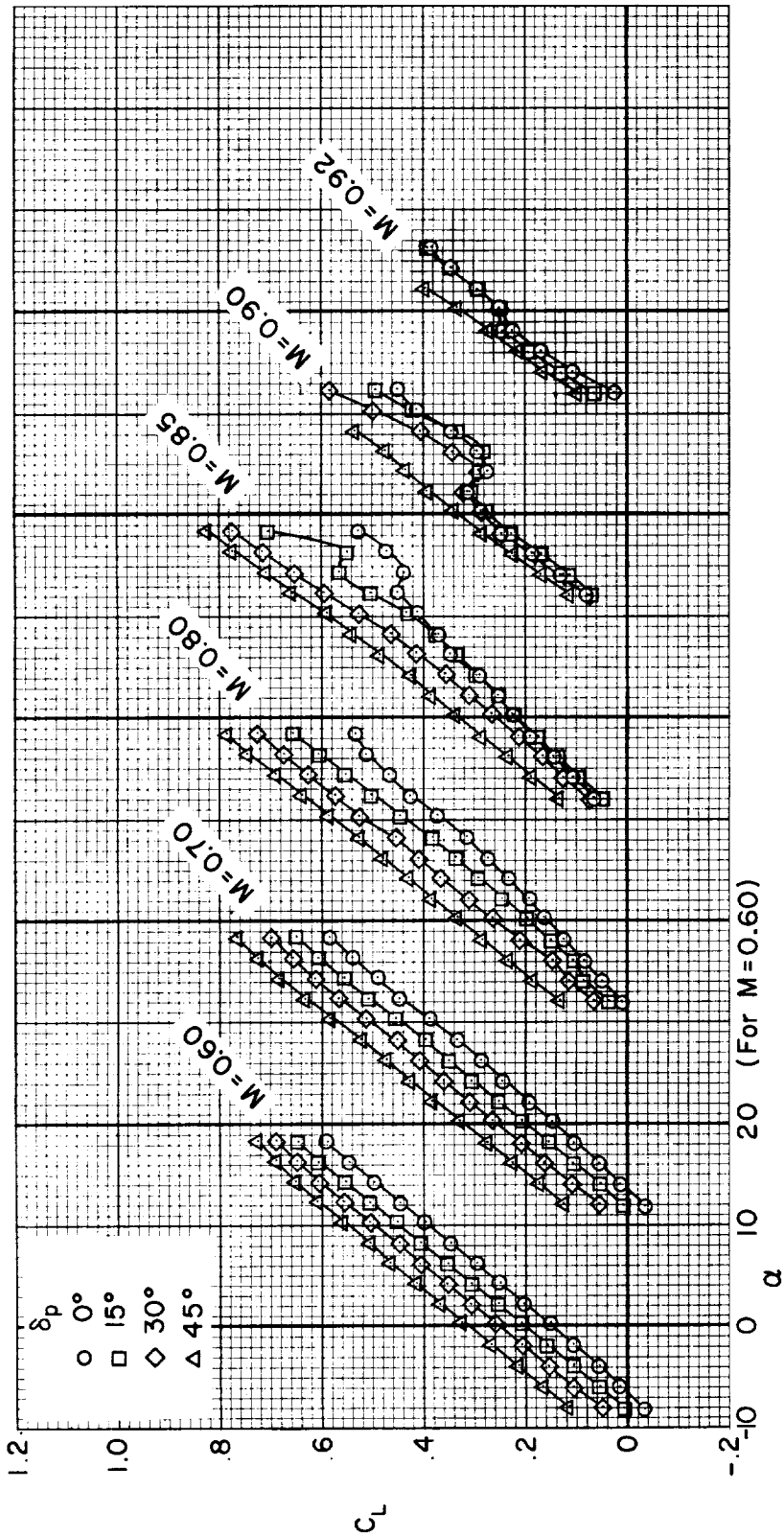

(a) Lift coefficient.

Figure 14.- The effects of pitch-flap deflection on the longitudinal characteristics of the model, elevons removed, for several Mach numbers; R = 5×10^6.

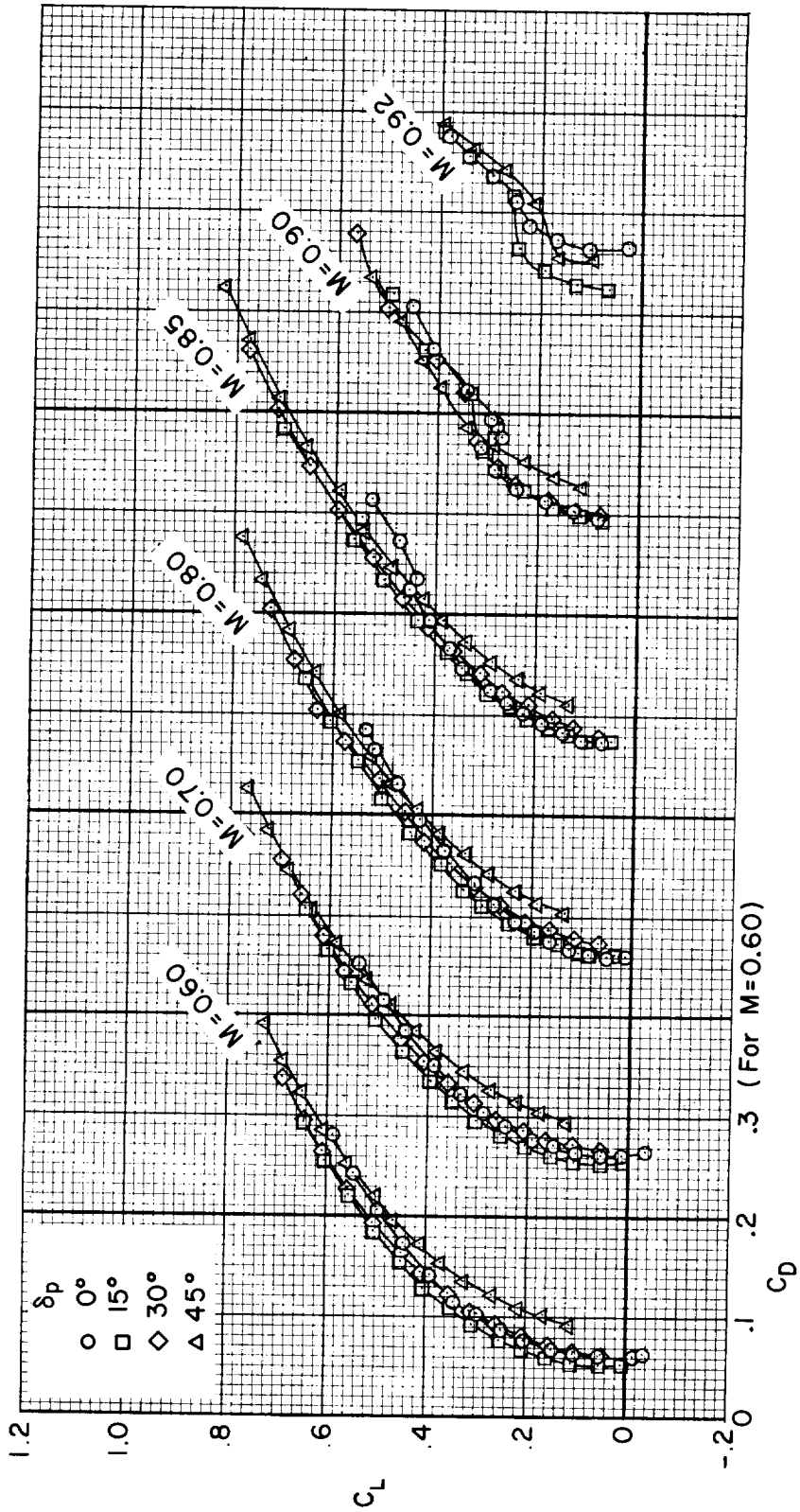

(b) Drag coefficient.

Figure 14.- Continued.

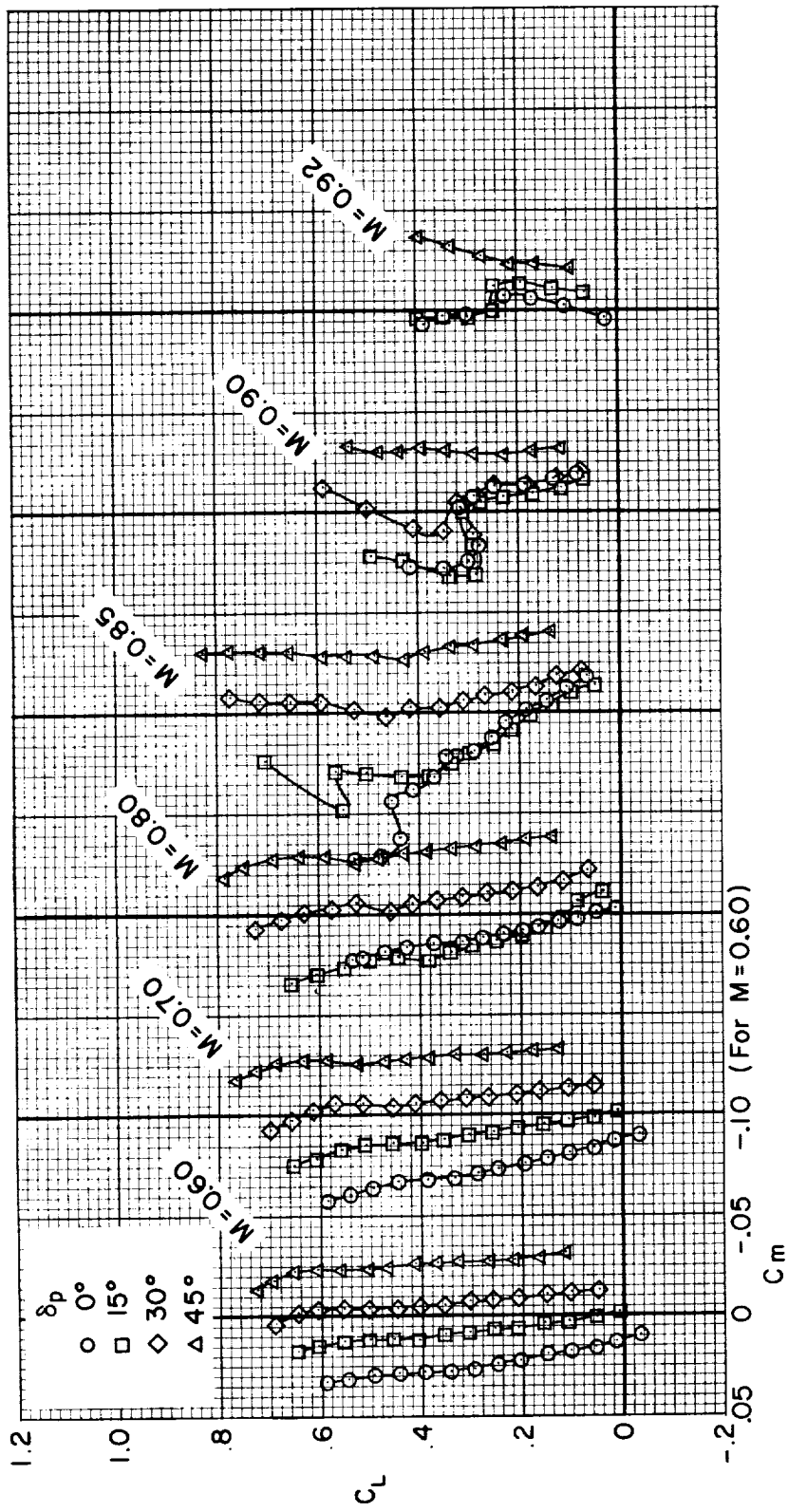

(c) Pitching-moment coefficient.

Figure 14.- Continued.

A
4
8
3

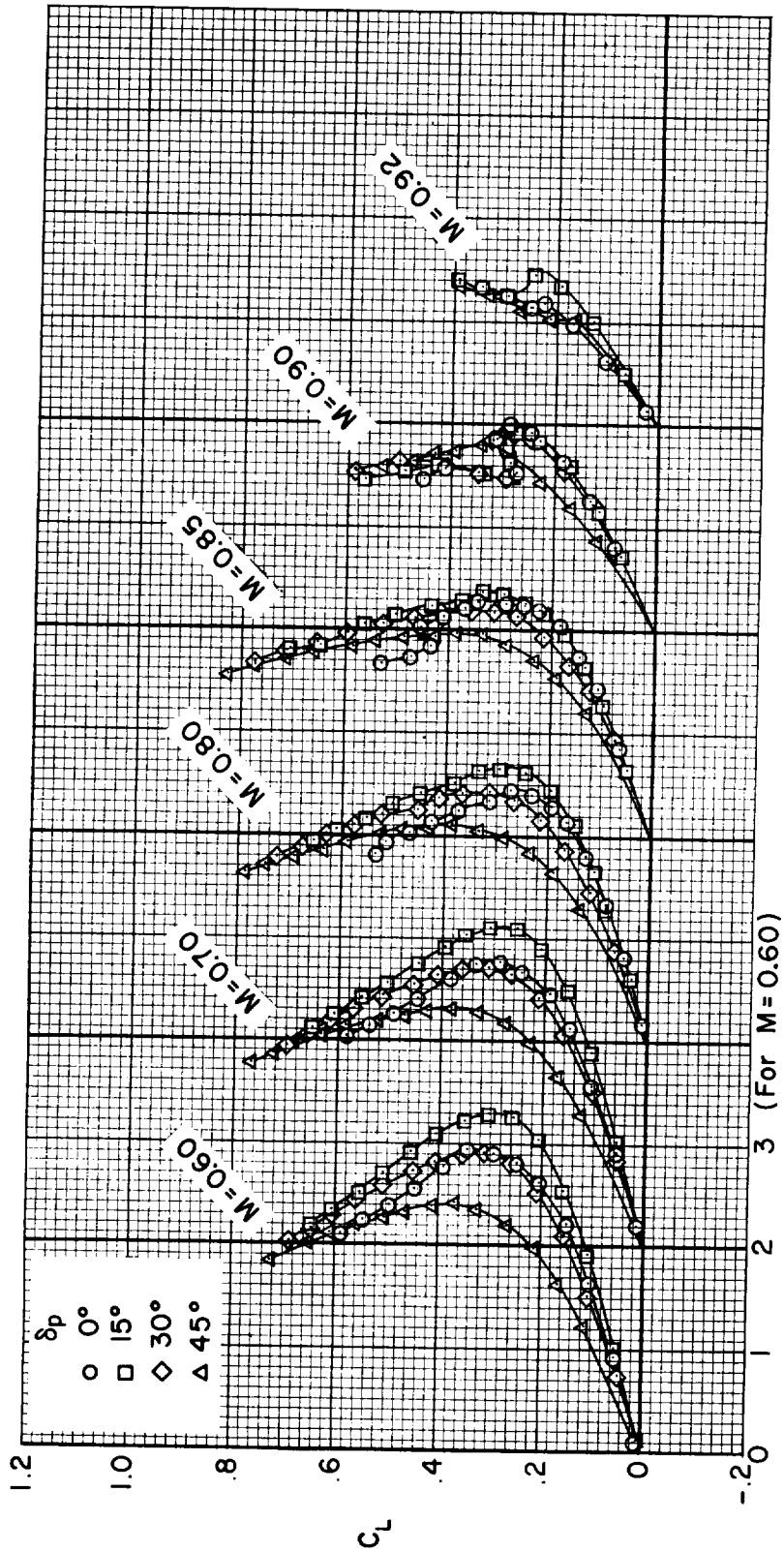

(d) Lift-drag ratio.

Figure 14.- Continued.

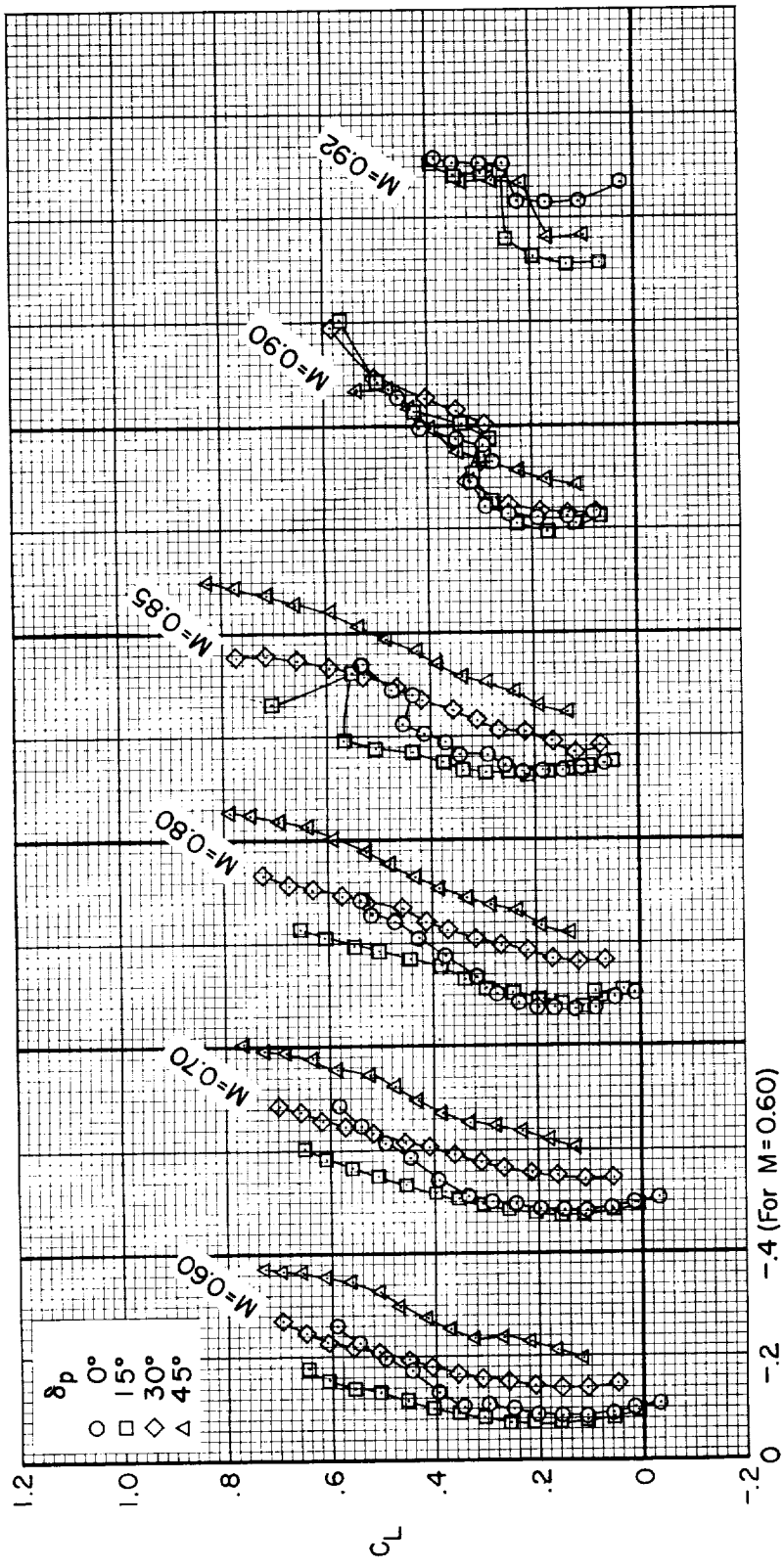

(e) Base-pressure coefficient.

Figure 14.- Concluded.

A 4 8 3

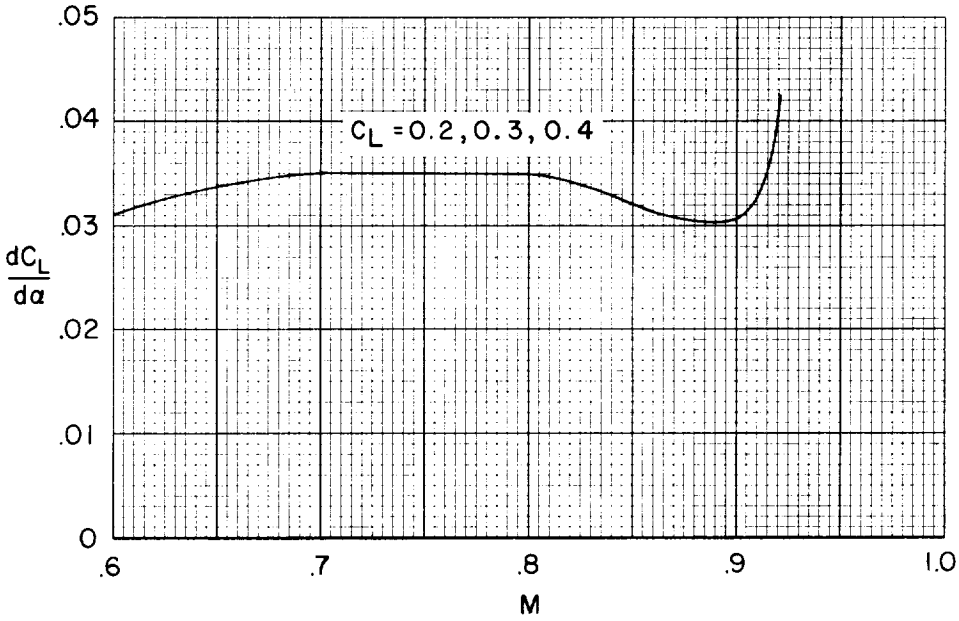

(a) Lift-curve slope.

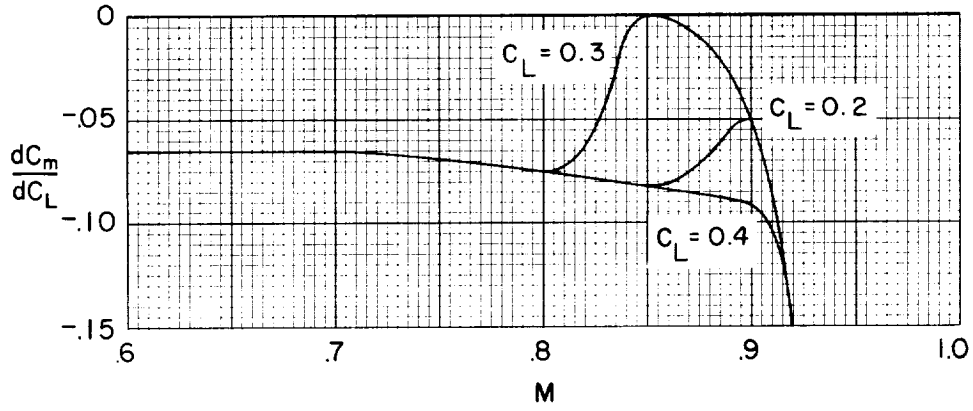

(b) Pitching-moment-curve slope.

Figure 15.- The effects of Mach number on the lift-curve slope, pitching-moment-curve slope, drag coefficient, lift-drag ratio, and lift coefficient for maximum lift-drag ratio; R = 5×10^6, $\delta_e = -10^\circ$, $\delta_p = 30^\circ$.

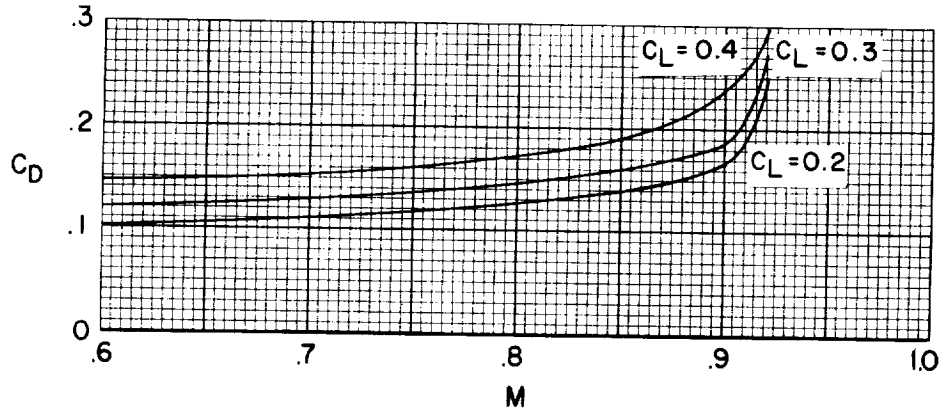

(c) Drag coefficient.

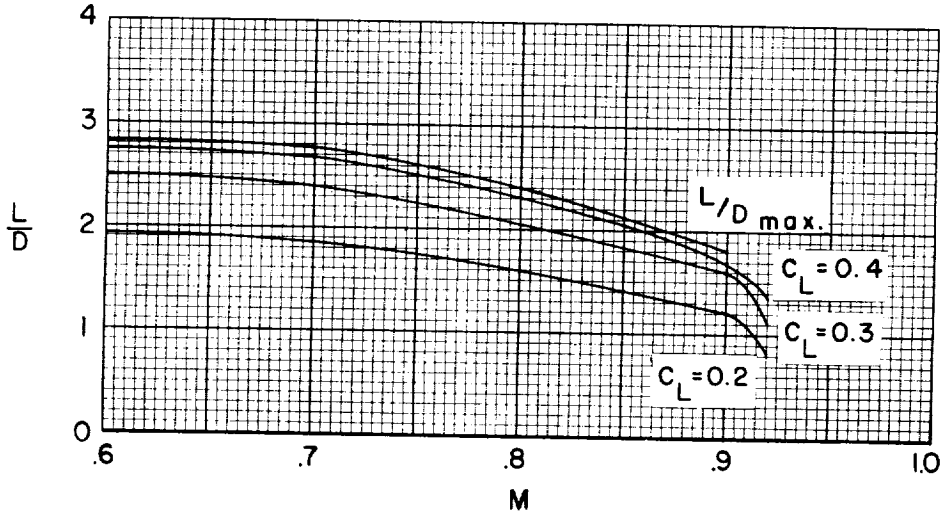

(d) Lift-drag ratio.

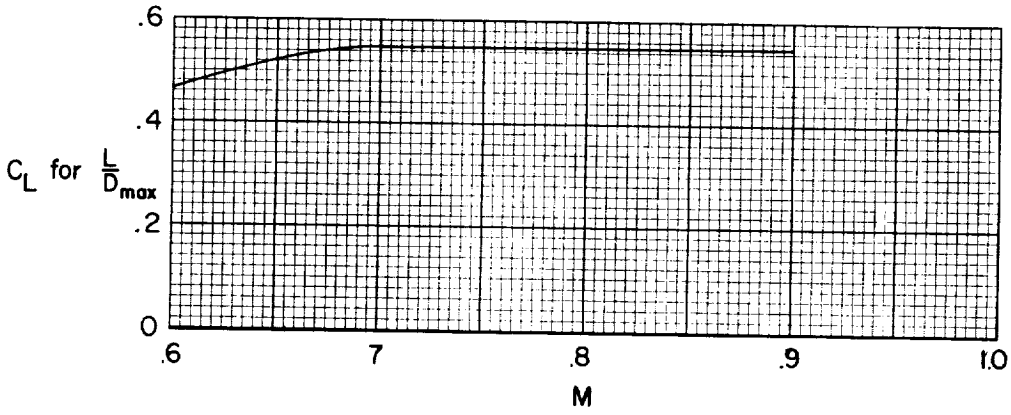

(e) Lift coefficient for maximum lift-drag ratio.

Figure 15.- Concluded.

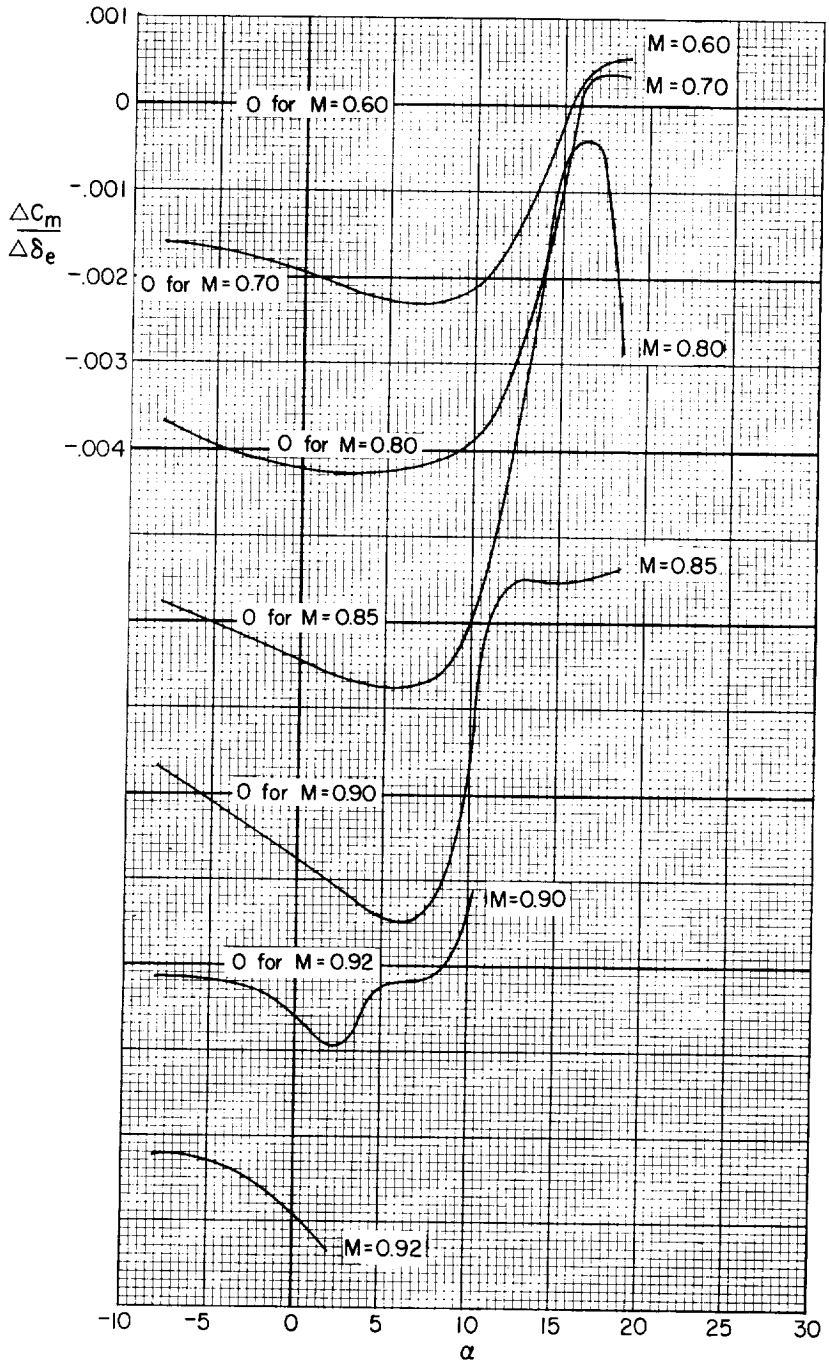

(a) Elevon effectiveness; $\delta_p = 30^\circ$.

Figure 16.- The variation with angle of attack of the control effectiveness of the elevons and the pitch flaps at several Mach numbers; $R = 5 \times 10^6$.

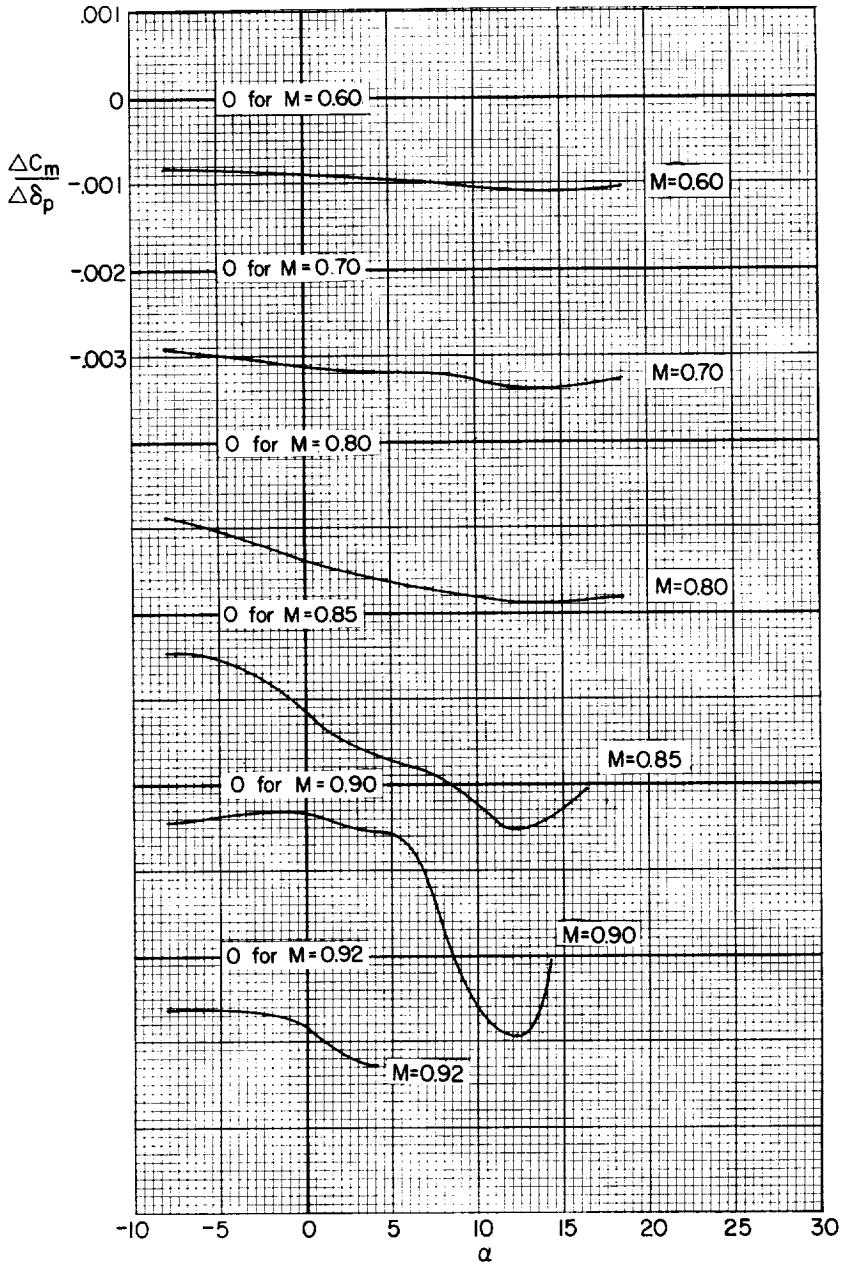

(b) Pitch-flap effectiveness, $\delta_e = -10^o$.

Figure 16.- Concluded.

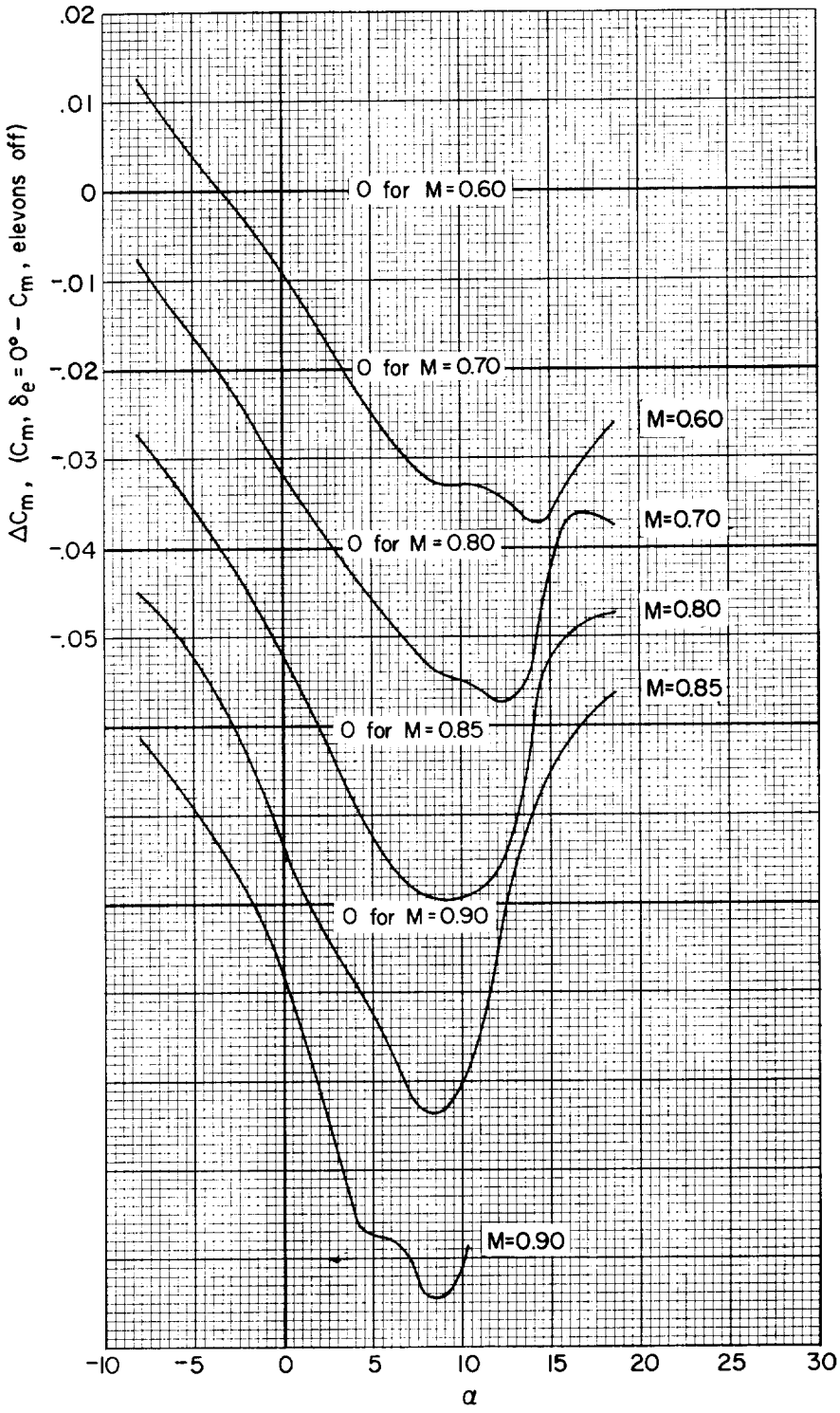

Figure 17.- The pitching-moment contribution of the elevons for several Mach numbers; $R = 5 \times 10^6$, $\delta_p = 30°$.

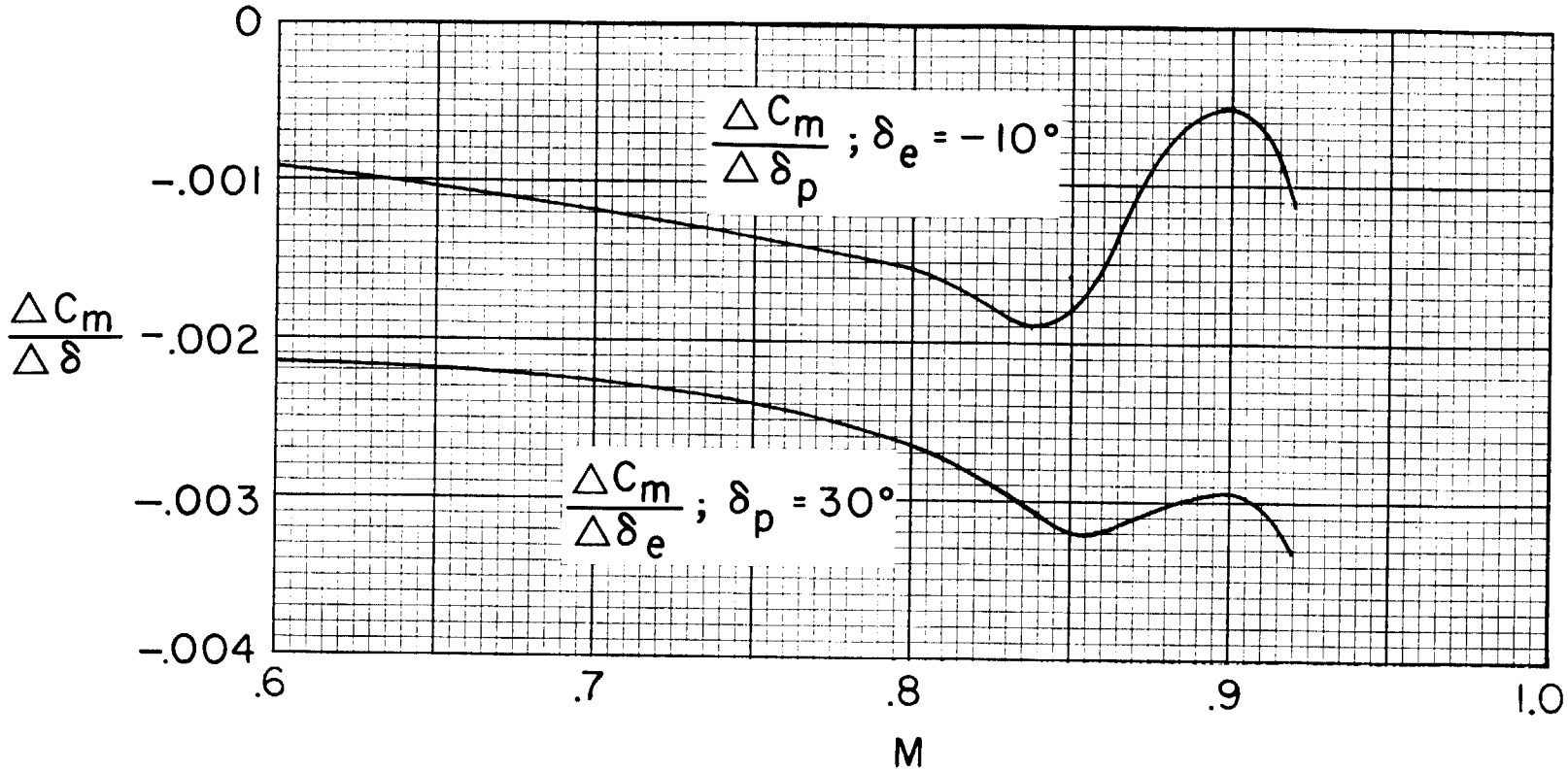

Figure 18.- The effects of Mach number on the longitudinal control effectiveness of the elevons and pitch flaps; $R = 5 \times 10^6$, $C_L = 0.30$.

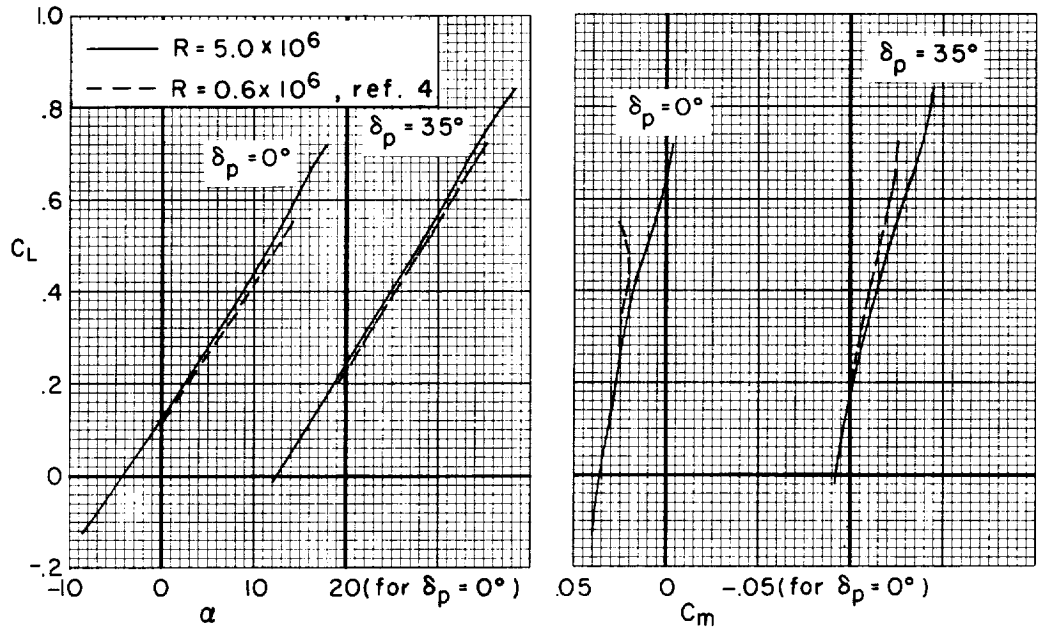

(a) M = 0.60, elevons on, $\delta_e = -10^\circ$.

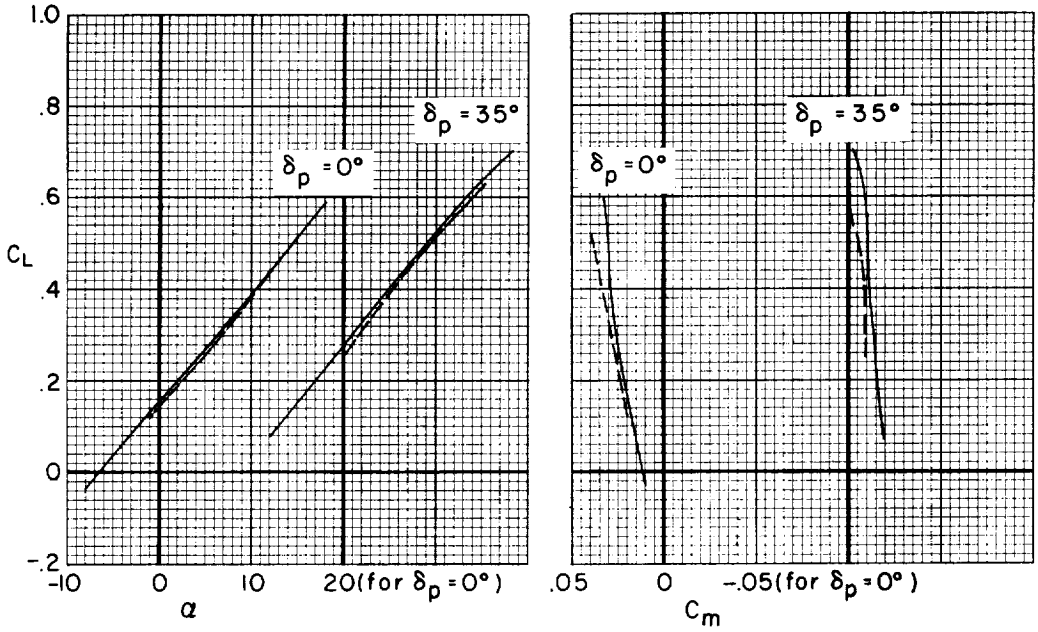

(b) M = 0.60, elevons off.

Figure 19.- A comparison of selected test results with the results obtained with a similar configuration reported in reference 4.

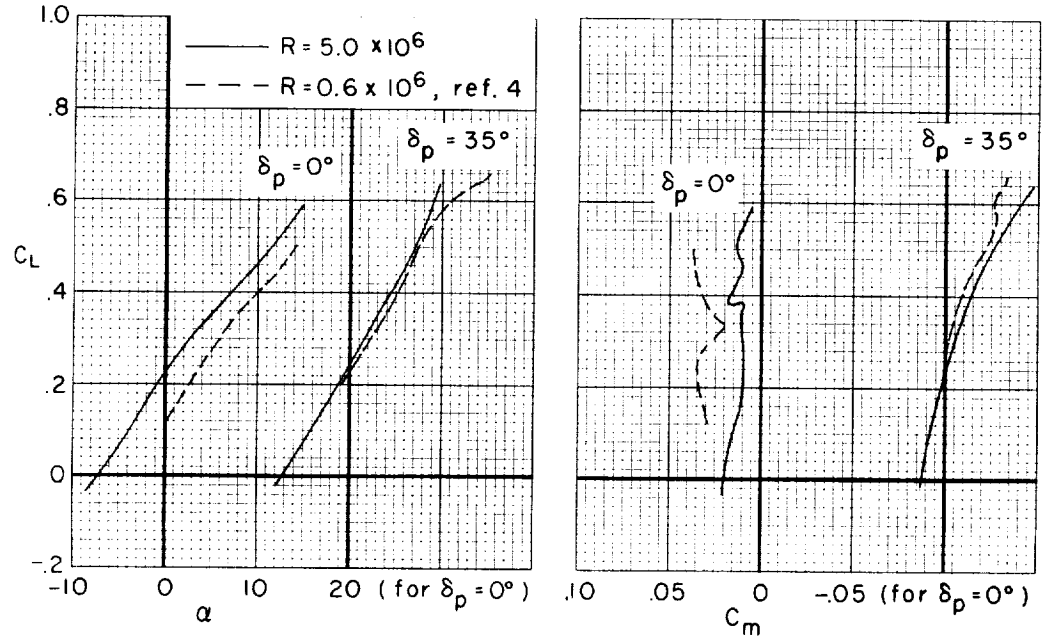

(c) M = 0.90, elevons on, $\delta_e = -10^\circ$.

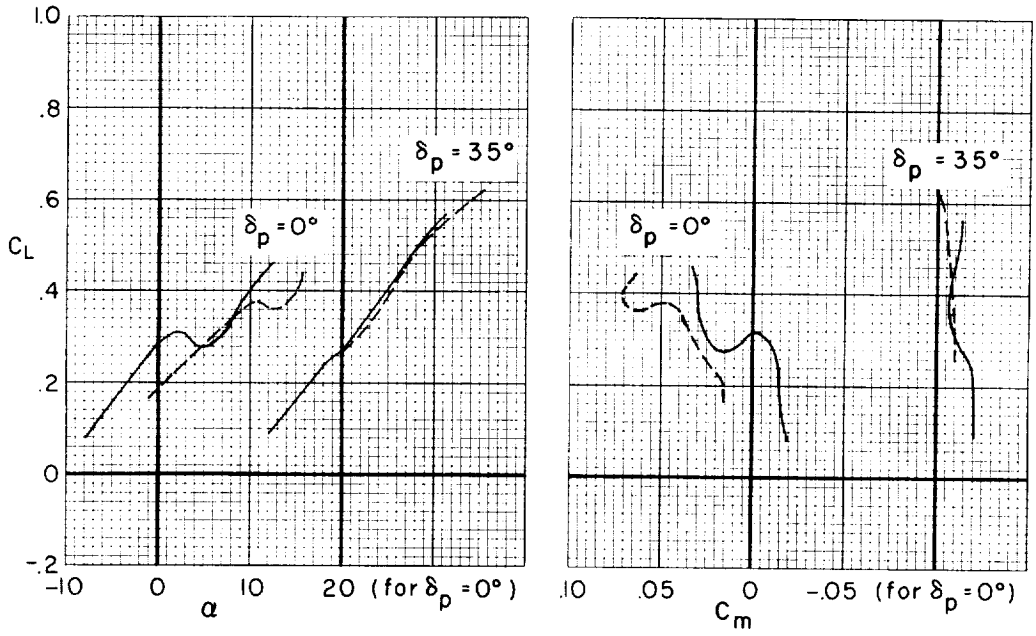

(d) M = 0.90, elevons off.

Figure 19.- Concluded.

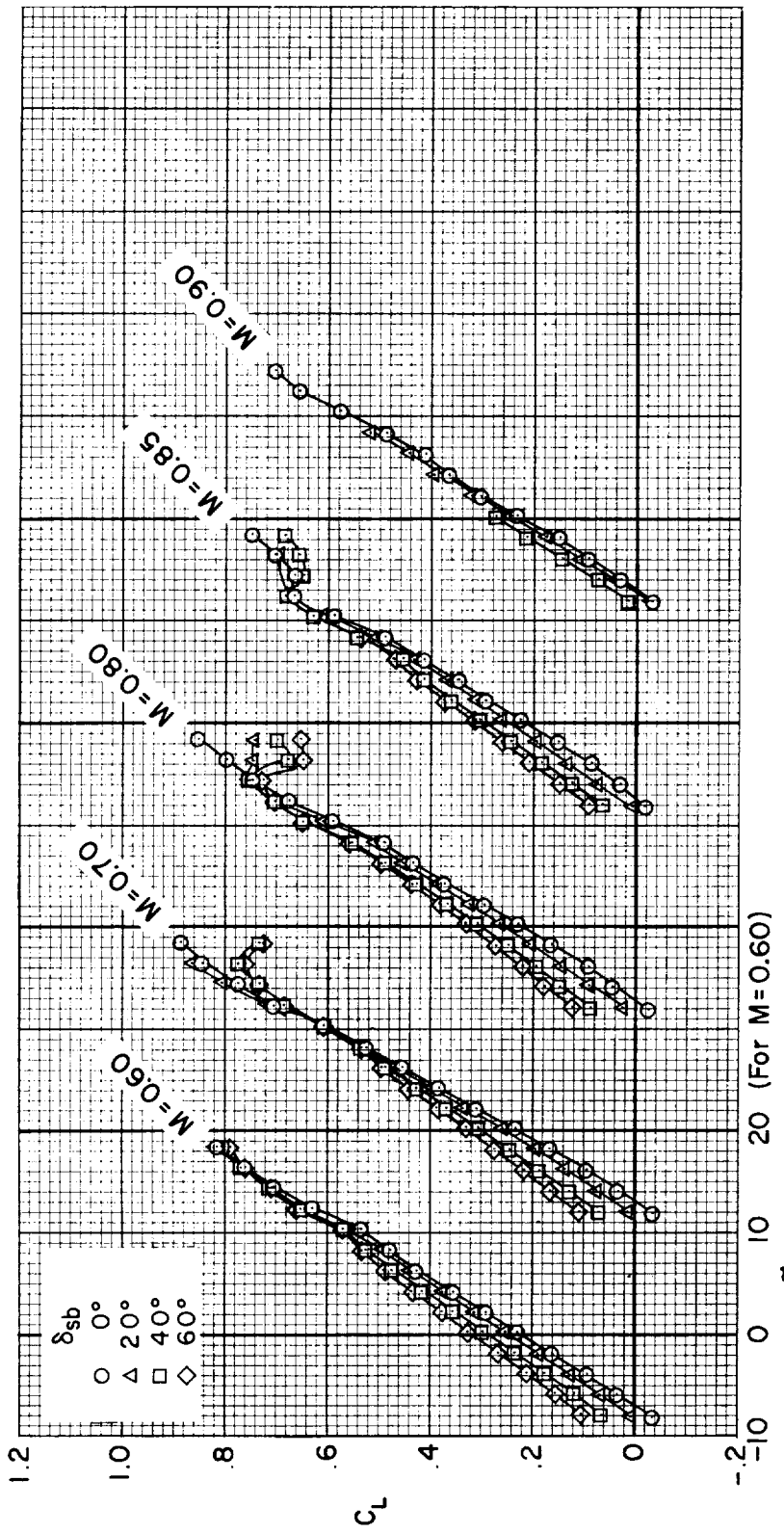

(a) Lift coefficient.

Figure 20.- The effects of speed brakes on the longitudinal characteristics of the model at several Mach numbers; $R = 5\times10^6$, $\delta_e = -10^o$, $\delta_p = 30^o$.

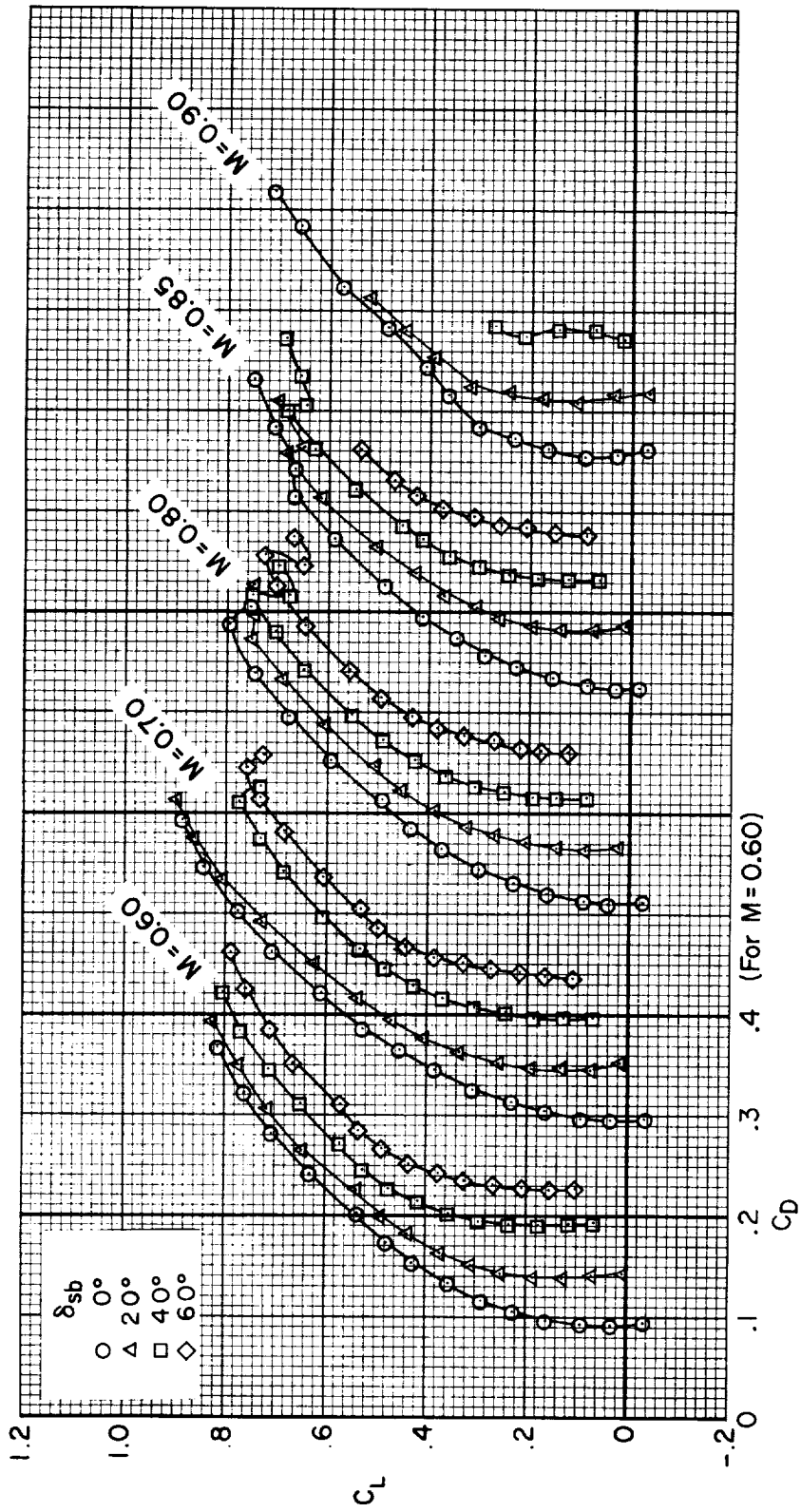

(b) Drag coefficient.

Figure 20.- Continued.

A
F
8
3

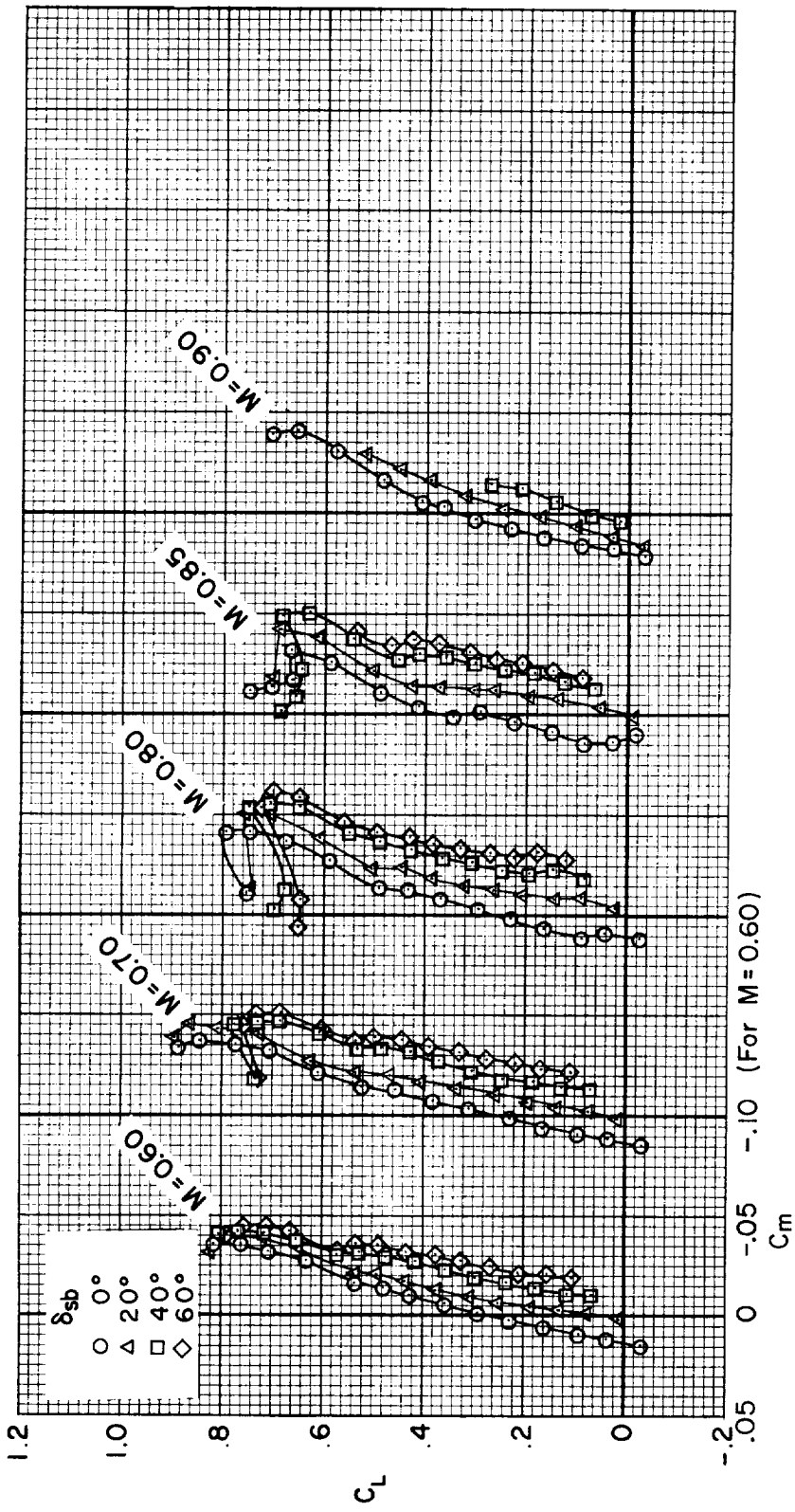

(c) Pitching-moment coefficient.

Figure 20.- Continued.

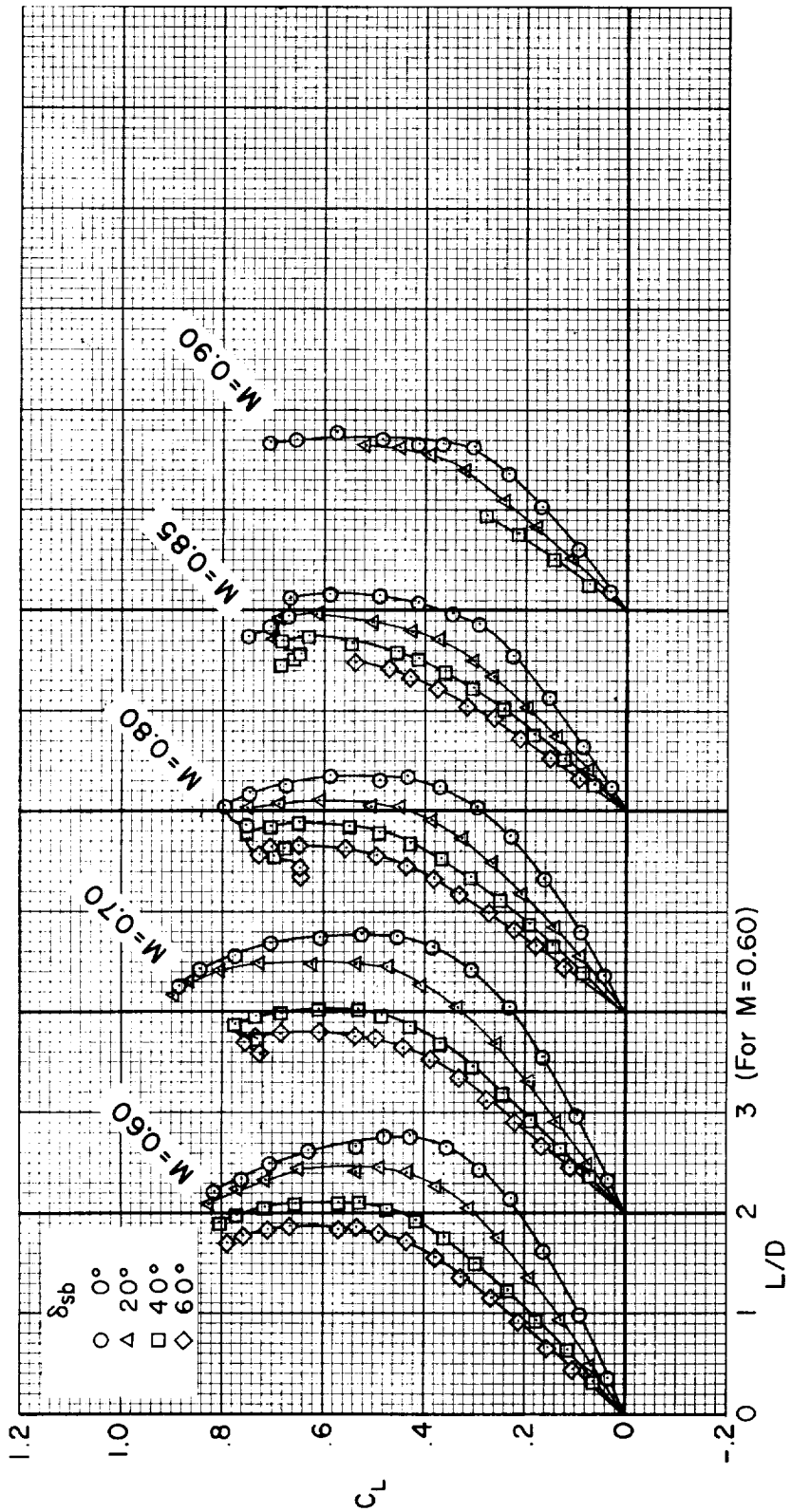

(d) Lift-drag ratio.

Figure 20.- Continued.

A 4 8 3

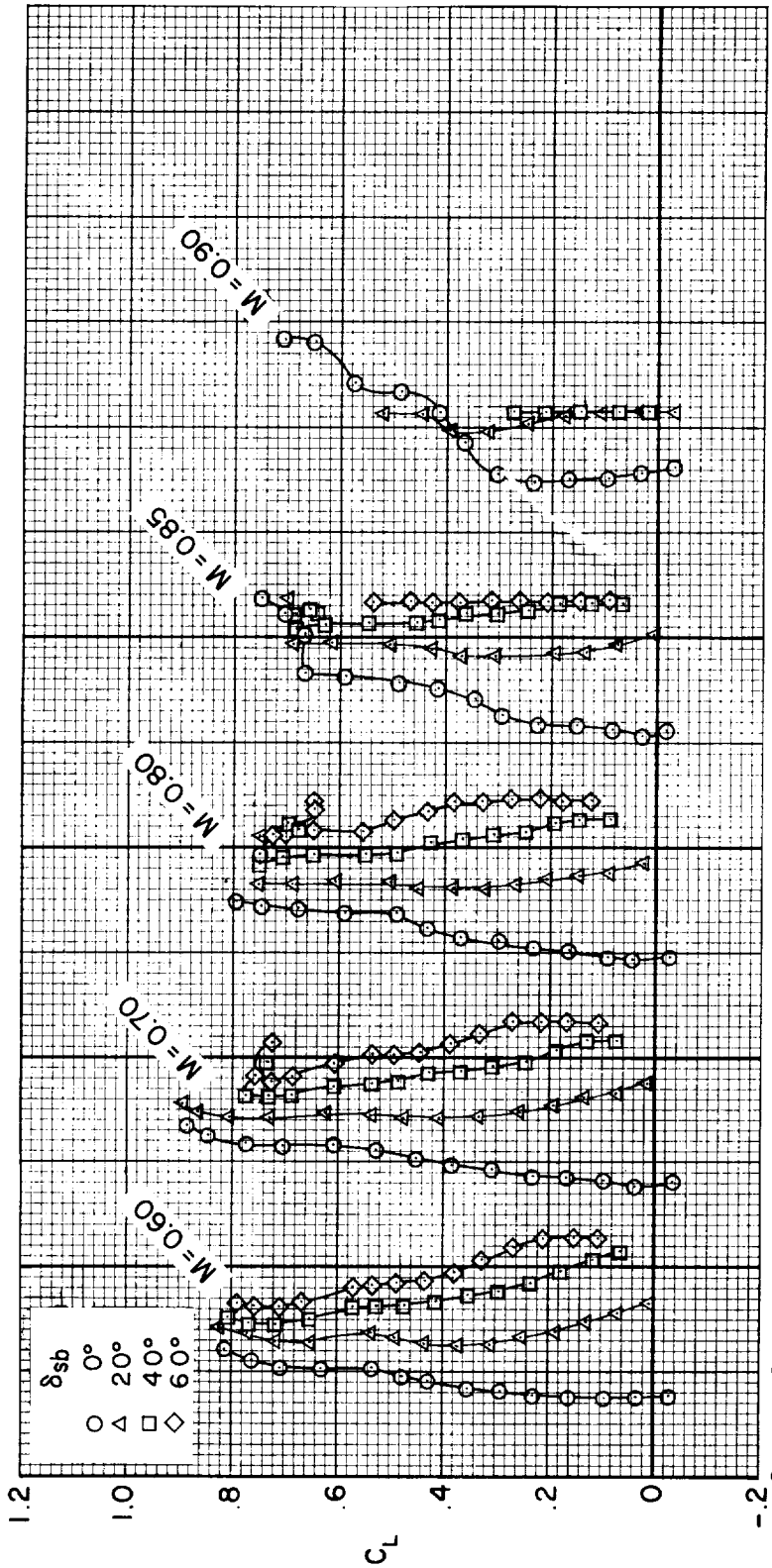

(e) Base-pressure coefficient.

Figure 20.- Concluded.

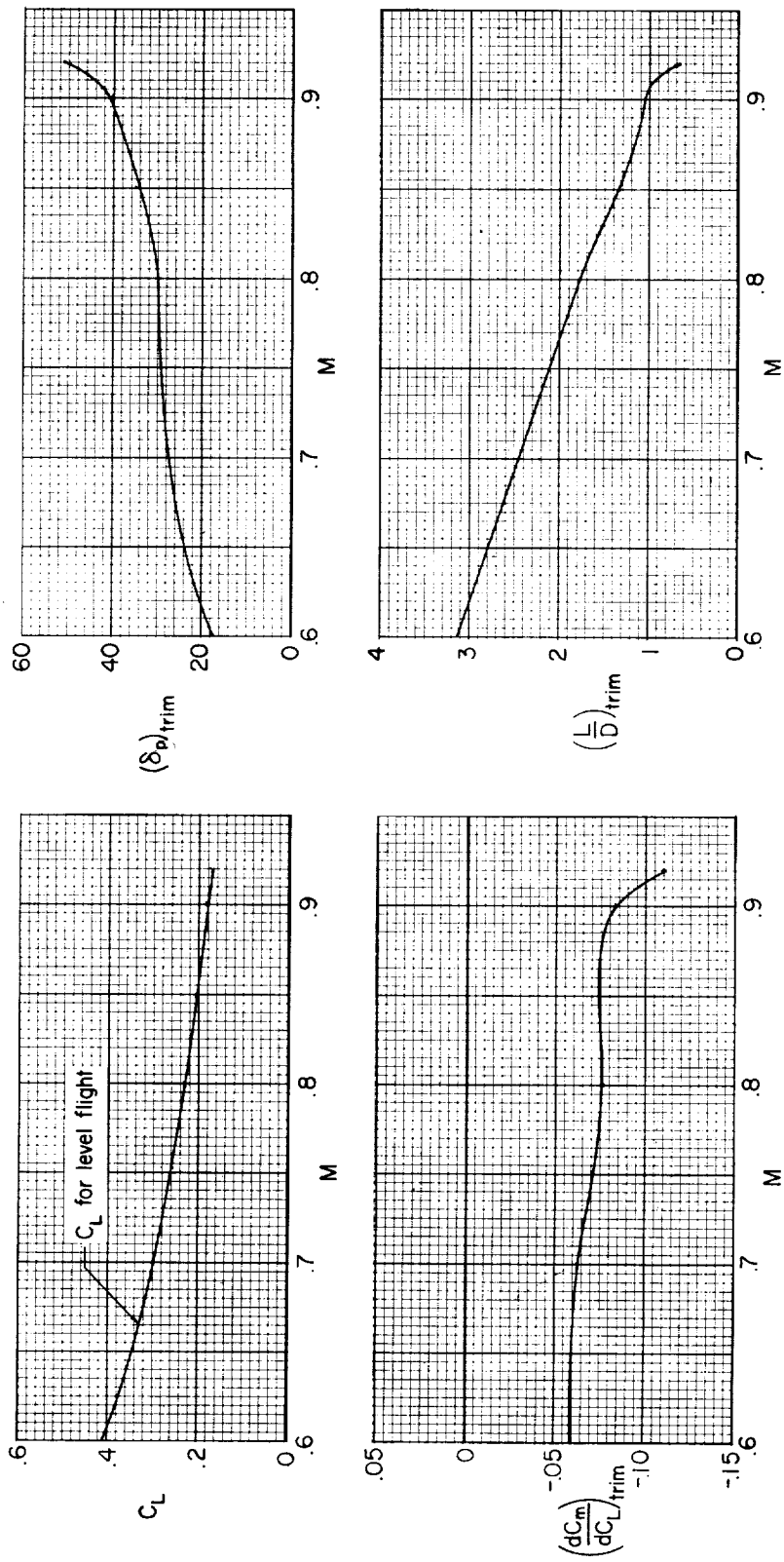

Figure 21.- The longitudinal characteristics of a hypothetical re-entry vehicle, having the model configuration, for steady level flight at 30,000 feet; $\delta_e = -10^0$, W/S = 65 lb/sq ft.

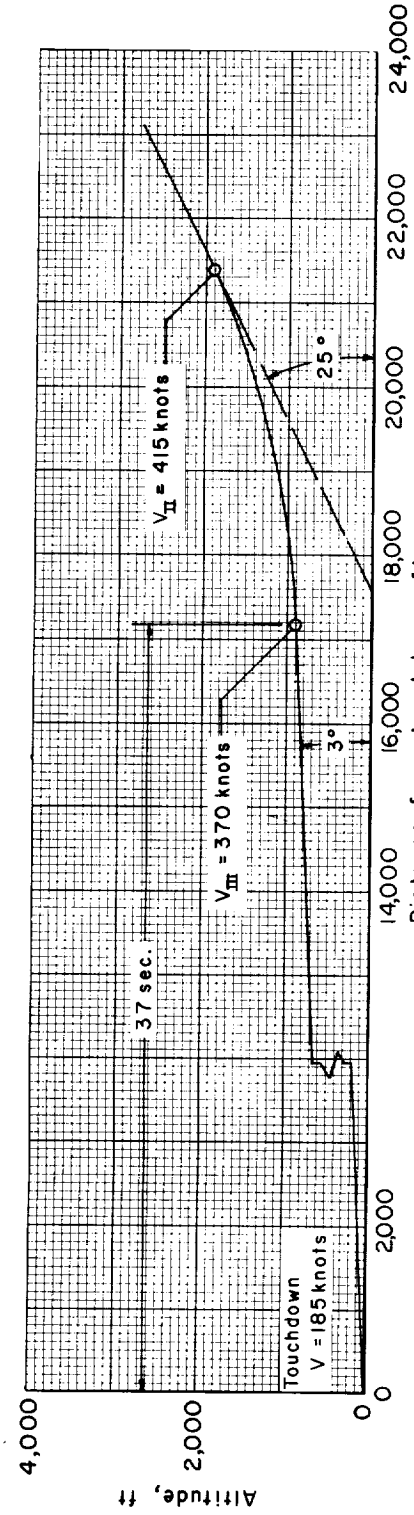

(a) "Optimum" pattern for the test airplane of reference 7.

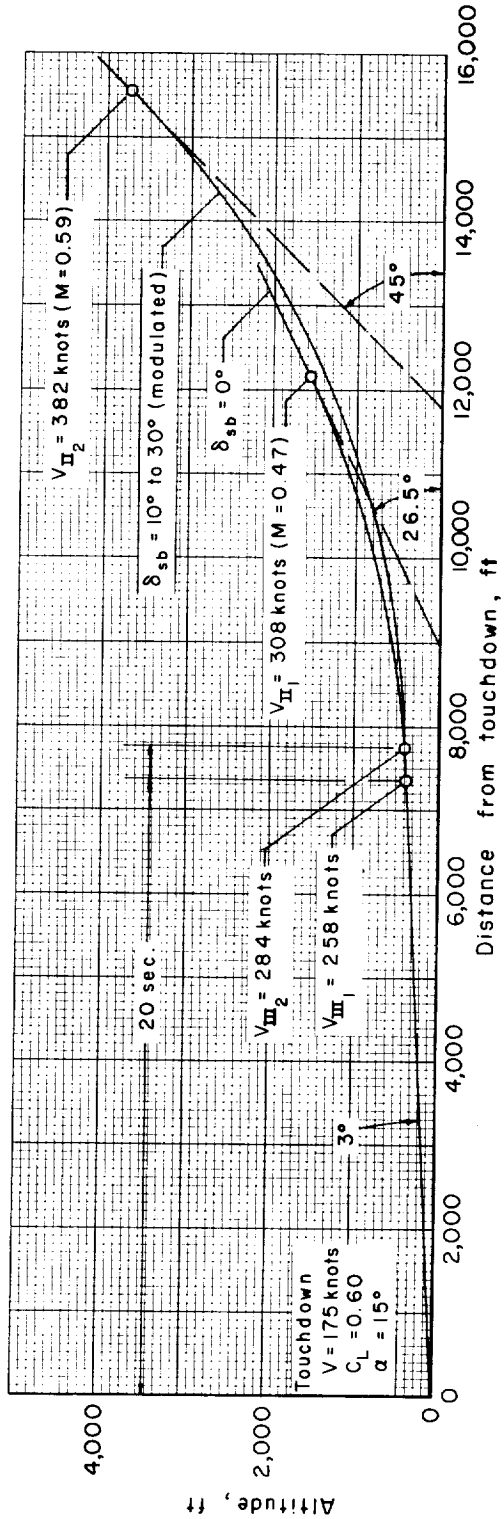

(b) Typical patterns for a hypothetical re-entry vehicle, with and without speed brakes extended.

Figure 22.- Landing-approach maneuver, calculated using the method of reference 7.